CHALMERS | GÖTEBORG UNIVERSITY

Coherent processes in

Superconducting quantum interferometers and qubits

JONN LANTZ

Akademisk avhandling som för avläggande av filosofie doktorsexamen i fysik vid Chalmers tekniska högskola och Göteborgs Universitet. Avhandlingen försvaras på engelska vid offentlig disputation fredagen den 12 april 2002, kl. 10.00 i FB-salen, Origovägen 1, Chalmers, Göteborg.

Fakultetsopponent är professor Christoph Bruder,
Departement Physik und Astronomie, Universität Basel.

Huvudhandledare är docent Vitaly S. Shumeiko.

Avdelningen för mikroelektronik och nanovetenskap
Chalmers tekniska högskola och Göteborgs universitet,
Göteborg, 2001

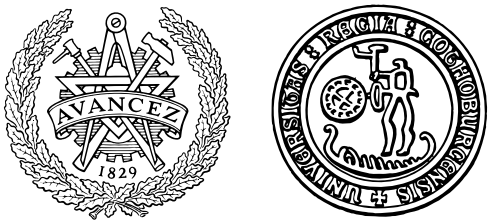

Coherent processes in

Superconducting quantum interferometers and qubits

Jonn Lantz

Department of Microelectronics and Nanoscience
Göteborg University and
Chalmers University of Technology

ABSTRACT

In this thesis we present theoretical investigations of the effects of Andreev bound states on the current transport in superconducting interferometers. We also investigate the slow dynamics of the Andreev states in a superconducting point contact, and the possible application as a quantum bit.

We consider superconductor-normal metal-superconductor (SNS) and normal metal- superconductor (NS) interferometers, where the contact region is a Y-shaped normal metal wave guide, and the two connection points to the same superconducting electrode can have different phases. The electric current in the interferometer is calculated as a function of the applied voltage and the phase difference ϕ. Andreev reflection in SNS and NS interferometers incorporates two features: interference in the arms of the Y-shaped normal region, and interplay with Andreev resonances. The latter feature yields rich phase dependent current structures in the subgap voltage region. The interference effect leads to a suppression of the current structures at $\phi = \pi$.

We investigate the effects on the Josephson current in NS interferometers due to current injection from the normal electrode. The two main effects of the nonequilibrium situation are: nonequilibrium population of the Andreev levels, which can result in enhancement, suppression, or even sign reversal of the Josephson current, and an anomalous interference Josephson effect, which gives rise to a long range Josephson effect, increasing with the voltage eV up to the superconducting gap Δ.

The two Andreev states in a superconducting quantum point contact can be accessed for manipulation and measurement by embedding the point contact in a superconducting loop. We calculate an effective Hamiltonian for the slow dynamics of the Andreev two-level system in the ring. Furthermore, we discuss methods of manipulation of the Andreev levels, and coupling of qubits. The state of the Andreev two-level system can be read out by monitoring the macroscopic quantum tunneling in a current biased Josephson junction, which is embedded in the superconducting ring of the qubit. We discuss the effects on the qubit, the readout scheme and the signal-to-noise ratio.

THESIS FOR THE DEGREE OF DOCTOR OF PHILOSOPHY

Coherent processes in

Superconducting quantum interferometers and qubits

JONN LANTZ

Department of Microelectronics and Nanoscience
Göteborg University and
Chalmers University of Technology

Göteborg, Sweden 2002

Coherent processes in superconducting quantum interferometers and qubits
JONN LANTZ
ISBN 91-628-5190-X

Department of Microelectronics and Nanoscience
Chalmers University of Technology
SE-412 96 Göteborg
Sweden
Telephone +46 (0)31-772 3189

Chalmersbibliotekets reproservice
Göteborg, Sweden 2002

LIST OF PUBLICATIONS

This thesis consists of an introductory part, four appended papers, referred to by Roman numerals in the text, and unpublished results discussed in Chapter 5. The appended papers are:

I. **Nonequilibrium Josephson effect in mesoscopic ballistic multiterminal SNS junctions**
P. Samuelsson, J. Lantz, V. S. Shumeiko and G. Wendin
Physical Review B **62**, 1319 (2000)

II. **Andreev resonances in quantum ballistic transport in SNS junctions**
Åke Ingerman, J. Lantz, E. Bratus, V. S. Shumeiko and G. Wendin
Physica C **352**, 77-81 (2001)

III. **Phase dependent multiple Andreev reflections in SNS interferometers**
J. Lantz, V. S. Shumeiko, E. Bratus and G. Wendin
Physical Review B **65**, 134523 (2002)

IV. **Flux qubit with a quantum point contact**
J. Lantz, V. S. Shumeiko, E. Bratus and G. Wendin
Physica C **368**, 315 (2002)

The order of the authors are indicative of each author's contribution to the work.

CONTENTS

CHAPTER 1

INTRODUCTION

Late in Camp 3, just below 6000m, on *Ruta Suecia* following the south west ridge on Aconcagua [1], 8 Jan 2001. We have just had our dinner (fillet of beef with Swedish mushroom sauce and pasta) and melted snow for the next day. There is no wind and it is *absolutely* quiet. The camp is placed at the col between cerro Piramidal and the great pillars. We have big walls on both sides. The east side is vertical and part of the well-known south wall, of which we from the camp cite only see the upper half. It looks cold, with blue-white snowfields and dark sandstone. The mountain forms a half circle, like an amphitheatre, around the dirty Glacier Francia and we are slowly climbing higher and higher on its western spur. Anders is sitting in the tent, listening to Chilean pop music on his am-receiver, while I am walking around waiting for the sunset in the Pacific Ocean and trying to get some nice pictures in the fading sunlight. The air is cold and dry. It is thin, but only in a good sense; clean and easy to breath. While the sun is fading through stripes of distant clouds, the shadows of the surrounding mountains are rising, creating strange visual effects on the sky. In the west are the youngest mountains, rocky peaks of which several are over 6000m high. When I look further to the east these jagged peaks turn into smooth sand hills, like a high altitude desert. In the far east, I can imagine the Pampas. Behind me is the is the great (nameless) pillar, a monolith in wind-polished sandstone, over two hundred meters high and probably never climbed. Tomorrow morning we will pack our stuff and climb an easy pitch to its base. Then we follow a ledge around it to find the way further up the mountain. Above the great pillar, there is still alpenglow on the south summit of Aconcagua, a sharp white edge.

1.1 MESOSCOPIC SUPERCONDUCTING JUNCTIONS

Mesoscopic physics concerns systems where the number of atoms is large, read macroscopic, but nevertheless the amplitude of the quantum mechanical fluctuations of some measurable quantity is comparable with its average, and the system cannot be treated classically. Hence, mesoscopic physics can be interpreted as the physics in the intermediate zone between quantum mechanics and Newtonian mechanics.

This thesis concerns electronic properties of simple superconducting circuits and,

in particular, different types of mesoscopic junctions between superconducting electrodes. These junctions can be of several types, having considerably different properties. The simplest type is the tunnel junction, or SIS junction (Superconductor-Insulator-Superconductor), where a tunnel barrier, usually a thin oxide layer, separates the superconducting electrodes. More complex is the family of SNS junctions, where N stands for Normal metal, *i.e.* a non-superconducting region. One may distinguish two main types of SNS junctions: junctions with a low concentration of impurities, where the transport is essentially ballistic and coherent, and junctions where the transport is diffusive. Metal or semiconductor junctions are usually diffusive. However, recent progress the semiconductor technology has made it possible to create essentially ballistic SNS junctions. We focus on this latter type of SNS junctions, and generally on junctions where the transport is coherent.

The theoretical story of superconducting junctions starts in 1957, when Bardeen, Cooper and Schieffer (BCS) presented their microscopic theory of superconductivity [2]. In early models of tunnel junctions a tunnel Hamiltonian was used to couple the two superconducting electrodes. This model was successfully applied by Cohen *et al.* [3] to calculate the dissipative current in voltage biased junctions. The most famous work was done by Josephson [4], who predicted a non-dissipative current in tunnel junctions, the Josephson effect.

When it comes to voltage biased junctions the tunnel Hamiltonian approach works well to calculate the lowest order process, single electron tunneling. This yields a current-voltage characteristics with zero dc-current at subgap voltages, $|V| < 2\Delta/e$, where Δ is the modulus of the superconducting order parameter. However, a finite dc-current onset at $V = \Delta/e$ was indeed seen in experiments by Taylor and Burstein in 1962 [5]. A few years later current structures at even lower voltages, $V = 2\Delta/ne,\ n = 1, 2, 3, ...$, where found [6, 7]. This *subharmonic gap structure* could not be explained by the simple tunnel Hamiltonian approach, which yields unphysical results for higher order processes (multi-particle tunneling) [8] due to the divergence of the BCS-density of states at the edges of the superconducting gap.

In 1963, de Gennes presented an equation of motion for quasiparticles in the superconducting state, today referred to as the Bogoliubov-de Gennes (BdG) equation [9, 10]. One year later Andreev, using arguments similar to the BdG-equation, suggested a new effect at the boundary between the normal and the superconducting state [11], later on referred to as *Andreev reflection*. The idea is that an electron, which is sent towards the surface of a superconductor, can be reflected as a hole. The conservation of current implies that two electron charges are transmitted into the superconductor during this process, which can be interpreted as that one Cooper pair [12] is added to the superconductor. The opposite process is also possible: An incoming hole is reflected as an electron, whereas a Cooper pair is emitted from the superconductor. In 1970 the Josephson effect in transparent SNS junctions was predicted by Kulik [13] and explained by coherent consequent Andreev reflections at the opposite NS interfaces. Generally, Andreev reflection is an important mechanism of current transport through NS interfaces, and a central concept in this thesis.

In the early works on the Josephson effect [13,14] an approach based on expansion over eigenstates of the BdG-equation was used. During the same period of years, several authors applied the Green's function technique to investigate the Josephson effect in SNS junctions [15, 16]. The Josephson effect in transparent constrictions, or ScS-junctions, was calculated in 1977 by Kulik and Omel'yanchuk [17], and in 1979 Artmenko *et al.* [18] extended this theory to voltage biased constrictions. A review of the Green's function techniques can be found in Ref. [19]

The theory for constrictions is consistent with the Landauer approach [20], widely used in the mesoscopic theory of normal junctions. The Landauer approach was applied to voltage-biased superconducting junctions for the first time in 1982 by Blonder *et al.* [21], who considered transport through a SIN-interface as a coherent scattering problem. This new approach was essentially to match solutions to the BdG-equation at the interface, in order to calculate *scattering states* for particles incoming from both directions. Knowing the probability current associated with the scattering states, it is straightforward to calculate the electrical current. Generally, the quantum mechanical BdG-Landauer approach is adequate for mesoscopic junctions, whose properties are dominated by coherent electron dynamics. The quantization of transverse electron modes in mesoscopic junctions also makes one-dimensional models appropriate [22, 23].

In 1982, Klapwijk *et al.* introduced the idea of multiple Andreev reflections (MAR) as the mechanism behind the ac-Josephson effect in voltage biased transparent SNS junctions [24]. The following year the theory was generalized to arbitrary transparency by Octavio *et al.* [25]. However, in these early papers about MAR the authors considered only incoherent transport in the normal region.

In the early 90:s several groups successfully calculated the dc-Josephson current in different kinds of mesoscopic weak links, using the quantum mechanical approach, [26–32]. It was shown that the bound Andreev states play an important role for the current transport in any kinds of superconducting junctions.

An important step was taken when the current-voltage characteristics for point contacts with arbitrary transparency was calculated, using the quantum mechanical approach and the Green's function approach [33–37]. The dc-part of the current in such junctions exhibits a staircase-like subharmonic gap structure with conductance peaks in the low voltage region ($eV < 2\Delta$), at $V = 2\Delta/en,\ n = 1, 2, 3, ...$ These current structures are explained by coherent MAR. The same subharmonic gap structure exists in tunnel junctions. However, in this case the subharmonic gap structure is suppressed; at small transparency $D \ll 1$ the amplitudes of the subharmonic structures decrease with the transparency as D^n

New fabrication techniques

The study of quantum junctions has attracted interest during the recent years, due to the developments in fabrication techniques. A very useful method to reach the quantum transport regime was developed in the beginning of the 90:s; the break junction tech-

nique [38–42]. The idea is to mechanically break a wire, in order to create a narrow constriction. Just before the wire breaks completely, the two electrodes can be linked only by a single atom, or even a chain of atoms [43]. Depending on the type of atoms in the point contact one may achieve a very low number of conducting modes, down to a single mode - a quantum point contact. It has been shown that the theory of coherent MAR in point contacts agrees with the experimental current-voltage characteristics with astonishing accuracy [44]. More recently, Koops *et al.* [45] have measured the non-sinusoidal current-phase relation of a nearly transparent point contact, in good agreement with the theoretical predictions [26–32]. The experiment was performed with a rf-SQUID-like setup, a superconducting loop with a point contact, where the induced flux through the loop was measured as a function of the applied external flux.

Furthermore, transparent normal regions have been fabricated with ballistic 2D-electron gas in a multi-layer semiconductor structure. With normal regions made with such 2D-electron gas, the mean free path of the electrons can reach several micrometers. The transport can be restricted to a small number of conducting electronic modes by using etched normal regions or by depositing electrostatic gates [26, 46]. Due to the large wavelength of the electrons in the 2D system (of the order of $10nm$) it is possible to create wave guides for the electrons with a low number of conducting channels. Hence, a finite length of the junction can be combined with the quantum transport regime.

SN and SNS interferometers

An interesting application based on mesoscopic SNS junctions is Andreev interferometry [47–49]. Essentially, an Andreev or NS interferometer consists of a three terminal device with two equipotential superconducting electrodes, having different superconducting phases, and one voltage biased normal electrode. The three electrodes are connected through an Y-shaped normal beam splitter (See Fig. 3.1). The central phenomenon in the NS interferometer is the phase dependence of the current in the normal electrode, due to interference effects on the Andreev transport through the double SN interface. Total suppression of Andreev reflection occurs when the phase difference is equal to π. If the two superconducting electrodes are connected to a superconducting ring, this phase difference can be controlled by means of the external magnetic flux through the ring. Flux-sensitive NS interferometers has been studied experimentally by several groups, see Refs. [50, 51].

An alternative setup is to replace the normal injection electrode with a third superconducting electrode, which gives an Y-shaped SNS junction or an SNS interferometer (see Fig. 3.6). Recently, Kutchinsky *et al.* discovered phase dependence of current structures at subgap voltages in diffusive SNS interferometers [52–55]. Although at present day no experiments have been performed with ballistic interferometers, one can generally expect even more pronounced phase dependent interference and resonant effects using junctions dominated by ballistic transport and preferably also in the quantum transport regime.

The effects of resonances associated with Andreev states in quantum SN and SNS interferometers are studied in Papers I-III. Paper I discusses NS interferometers while Paper III, and part of Paper II, is devoted to the phase dependent subharmonic gap structure in voltage biased SNS interferometers.

Nonequilibrium Josephson effect

It is generally accepted that bound Andreev states play an important role for the electronic transport in mesoscopic SNS junctions [14]. Each transport mode in a SNS junction is associated with a number of Andreev levels, which depends on the effective length L of the normal region roughly as $N \sim \xi_0/L$. Short junctions, on the scale of the superconducting coherence length $\xi_0 = \hbar v_{\rm F}/\Delta$, host only one pair of levels, while the number of levels in long junctions may be large. The Josephson current in long junctions decays exponentially with increased length [13, 16], which is due to the fact that the Andreev levels carry current in alternate directions and therefore tend to cancel out each others current contributions pairwise [56]. This cancellation depends on the population of the Andreev levels, which in equilibrium is the Fermi distribution. By using the interferometer setup, and injecting electrons into the normal region from the probe, it is possible to create a nonequilibrium population of the Andreev levels and hence to modify the Josephson current.

In Paper I we give a detailed description of the nonequilibrium Josephson effect in quantum 3- and 4-terminal devices, *i.e.* quantum SNS junctions with one or two probes attached to the normal region. The focus is put on the anomalous Josephson current [57]. The origin of this effect is an asymmetry between the nonequilibrium Josephson current produced by injected electrons and injected holes. The anomalous current does not depend on the length of the normal region and can be of the order of the equilibrium current in a point contact, even if the junction is long and the equilibrium current is exponentially small.

1.2 QUANTUM ELECTRONICS

In 1986 Leggett [58] suggested that a macroscopic quantum two-level system could be achieved using a superconducting ring with a tunnel junction, *i.e.* an rf-SQUID. His idea was that a hysteretic rf-SQUID biased at a half flux quantum, $\Phi_0/2$, where $\Phi_0 = \hbar/2e$, should fluctuate quantum mechanically between two states with persistent currents in opposite directions, required that the charging energy of the junction is sufficiently small, $E_C = (2e)^2/2C$. The device was suggested as a tool for studying macroscopic quantum mechanics, and also the role of dissipation [59]. If the two-level system is well separated from higher energy levels, the system can be seen as an artificial spin-1/2 particle in an effective magnetic field, which depends on the electronic properties of the device and the external flux. In order to measure the spin-state of such a device a quantum measurement is needed, *i.e.* the meter should have sufficient accuracy to distinguish the two states from each other. Leggett's suggestion was to

use a dc-SQUID, inductively coupled to the rf-SQUID, to measure the induced flux by the rf-SQUID. The amplitude of the signal from the rf-SQUID is of the order of a flux-quantum. Generally, the coherence in mesoscopic two-level systems is extremely sensitive to environmental noise. The hysteretic rf-SQUID is unfortunately strongly coupled to noise in the external flux, due to the large inductance. This is probably the reason why the early attempts to observe the effect have failed. However, promising experiments has recently been reported by Friedman *et al.* [60].

The idea of quantum computing* has brought back Leggett's two-level system to the limelight. The basic building block in a quantum computer is the qubit, or QUantum BIT, which is a quantum two-level system. The qubit corresponds to the ordinary bit in classical computers, but there are some important differences. The state of the qubit can take any superposition of 1 and 0, compared to the discrete values of the ordinary bit. Moreover, this superposition is coherent which implies an additional degree of freedom; the phase difference between the two eigenstates.

Several groups explore the possibility of microscopic qubits, *i.e.* qubits based on individual microscopic degrees of freedom, for example nuclear spins in molecules (NMR) [62, 63]. However, we will focus on macroscopic superconducting qubits, which open the possibility for coherent quantum electronics. Several promising experiments on superconducting qubits have been based on phase degree of freedom in Josephson junctions. Usually one distinguishes between *charge qubits*, working in the regime $E_C \gg E_J$ [64–66], and *flux qubits*, working in the regime $E_J \gg E_C$ [58, 60, 67], where $E_J = \Phi_0 I_c/2\pi$ is the Josephson energy. For a review see Ref. [68].

Quantum coherence in a qubit based on the Josephson effect was demonstrated for the first time in 1999 by Nakamura *et al.* [65]. They showed that coherent oscillations between two charge states of a Cooper pair box [64], *i.e.* a small island connected via a Josephson junction to a superconducting reservoir, could be induced by voltage pulses. More recently Vion *et al.* [69] reported measurements of Rabi-oscillations on a similar charge qubit with a significantly longer decoherence time, $T_\phi \sim 0.5\mu s$, compared to the experiment of Nakamura *et. al*, $T_\phi \sim 2ns$. The hysteretic rf-SQUID by Leggett is an example of a phase qubit. A similar design has been studied by Mooij *et al.* [67], who constructed a flux qubit in the non-hysteretic regime $E_J \ll E_L = (\Phi_0/2\pi)^2/L$, where L is the geometric inductance, to avoid the sensitivity to external flux noise. All these qubits are children in the recent baby boom of superconducting qubits, and new ideas are still coming.

All qubits based on the Josephson effect use large classical Josephson junctions, where the phase difference is the only dynamical variable. An alternative approach is to use the inherent dynamics of the bound Andreev states in a quantum junction, which is not directly related to the dynamics of the phase difference. In a quantum point contact with a single conducting channel there is only a single pair of Andreev levels, which is a good candidate for the qubit application. The state of the Andreev

*This thesis does not concern any quantum computing, although this is an interesting subject. We are only considering the basic building block; the qubit, which is interesting enough on its own. The theory and algorithms of quantum computing can be found for example in [61].

two-level system determines the direction of the persistent current in the contact. If the two electrodes of the point contact are connected, forming a superconducting ring the situation becomes similar to Leggett's bistable rf-SQUID, with the difference that the inductance of the ring can be low, $E_L \gg E_J$. (The Josephson energy of a transparent quantum point contact is of the order of the energy gap $E_J \sim \Delta$.) Although the Andreev level qubit is a phase qubit, it is not the phase difference which is the relevant degree of freedom, but the state of the Andreev two-level system of the point contact. Thus, this device can be seen as a microscopic qubit, which is coherently coupled to the macroscopic ring.

Paper IV discusses a qubit based on the Andreev two-level system. The dynamics of the qubit is discussed in Sec. 2.1 and Chapter 4.

Measurement of persistent current qubits

The spin-state of a qubit based on the Josephson effect can be measured by means of the charge on a junction or the supercurrent, which is a function of the phase difference. Since the classical meter is a source of noise, a weak coupling between the meter and the qubit is required, which obviously makes the measurement process increasingly difficult due to the small signal from the qubit. Hence, great effort is put on the design of accurate methods to measure charge [70, 71] and flux, see [60, 67]. A new meter to measure persistent currents has recently been developed by Cottet *et al.* [66], with promising experimental results [69]. The technique is applicable to the phase or charge qubits where the two-level system couples to the persistent current in a superconducting ring. Hence, these systems can also be measured using the dc-SQUID technique. The new meter by Cottet *et al.* is a Josephson junction with large critical current compared to the typical current states, which is embedded in the superconducting ring. The big Josephson junction is also connected to a stable current source and a voltmeter. The measurement is performed by increasing the current bias from zero to a peak value where the rate for macroscopic quantum tunneling (MQT) in the meter is significant. The MQT-event yields a voltage pulse, which can be measured by the voltmeter. The rate for MQT depends strongly on the current through the junction, and hence on the direction and amplitude of the current in the ring, which can be used to determine the current state of the qubit.

The main advantage of this MQT-meter compared to the dc-SQUID is that it measures the current state rather than the induced flux, which is a weak effect if the qubit is operated in the non-hysteretic regime $E_L \gg E_J$.

In Sec. 5.1 we discuss a qubit with persistent current states, connected to a MQT-meter. The general properties of the qubit-meter system are discussed as well as the signal-to-noise ratio of measurements at zero temperature.

1.3 OUTLINE OF THIS THESIS

This thesis is to large extent a study of different aspects of nonequilibrium Andreev states.

The structure of the remaining part of this thesis is as follows.

In Chapter 2, I introduce the formalism on which the work is based. We use a quantum mechanical scattering approach to calculate current-voltage characteristics and the (non)equilibrium Josephson effect in quantum SNS junctions. The dynamics of the Andreev states in a point contact is investigated using a functional integral approach.

In Chapter 3, I present the results of Papers I-III. In these papers we discuss NS and SNS interferometers and the effects of the Andreev bound states on the current-voltage characteristics. We also discuss the nonequilibrium Josephson effect caused by normal injection in an SNS junction.

In Chapter 4, I present the results of Paper IV and discuss the Andreev level qubit. The paper is devoted to the slow dynamics of the Andreev states in a quantum point contact and the possible qubit application. Manipulation of the qubit state and coupling of qubits are other subjects in the discussion.

Finally, in Chapter 5, I discuss the readout scheme of superconducting qubits, using the method developed by Cottet *et al.* [66]. The method may in particular be useful for experiments with Andreev level qubits.

CHAPTER 2

SUPERCONDUCTING JUNCTIONS

In this chapter I will introduce the formalisms which are used in the appended articles. Although three of the four appended papers are based only on the scattering theory I find it illustrative to begin with the functional integral approach to the point contact, the results of which are used to describe the Andreev level qubit. The functional integral approach gives an overall picture of the junction in the electric circuit, including the effective capacitance of the junction and the influence of inductive and capacitive elements in the circuit. The scattering approach, which is introduced in Sec. 2.2, concerns only the transport properties of the junction, and implies the phase difference being a well defined classical variable.

2.1 FUNCTIONAL INTEGRAL APPROACH TO THE QUANTUM POINT CONTACT

In this section we use the functional integral technique to calculate an effective Hamiltonian for the quantum point contact, describing the dynamics of the energy levels close to the Fermi surface. Our aim is to describe the dynamics of the Andreev two-level system in a fluctuating environment. We also derive the Hamiltonian describing the slow phase dynamics of the tunnel junction.

Hamiltonian of the superconducting quantum point contact

It has been shown by Levy Yeyati *et al.* [72] and Cuevas *et al.* [36] that the Josephson effect in superconducting quantum constrictions with arbitrary transparency can be described using a tunnel Hamiltonian description of the coupling of the electrodes. We can write the Hamiltonian for a single-mode quantum point contact connecting two bulk electrodes as

$$H = H_L + H_R + H_T + H_Q, \tag{2.1}$$

which consists of the following terms. The bulk electrodes are described by the Hamiltonian for the BCS-superconducting state [2], considered in the mean field approxima-

tion (see *e.g.* [73] for a detailed derivation); for the left electrode,

$$\hat{H}_L = \int_{r\in L} d^3r\, \hat{c}_L^\dagger(r,t)\left[\left(\frac{-\hbar^2}{2m}(\vec{\nabla}-\frac{ie}{\hbar}\vec{A})^2-\mu\right)\sigma_z+\hat{\Delta}_L\right]\hat{c}_L(r,t), \tag{2.2}$$

where $c(r,t) = (\psi_\uparrow(r,t), \psi_\downarrow^\dagger(r,t))$ is the two component Nambu representation for electrons and holes in the superconductor, σ_i denote the Pauli matrices, and the order parameter matrix is given by the equation,

$$\hat{\Delta}_L = \Delta_L e^{i\chi_L(r,t)\sigma_z}\sigma_x, \tag{2.3}$$

where Δ_L is real and positive. The bulk Hamiltonian for the right electrode is similar. Using the mean field approximation we neglect fluctuations of the magnitude of the order parameter Δ_L and also deviations from the Josephson relation,

$$eV(t) = \frac{1}{2}\hbar\dot{\phi}(t), \tag{2.4}$$

where $V(t)$ is the voltage across the point contact and $\phi(t) = \chi_R(r_T,t) - \chi_L(r_T,t)$ the phase difference across the point contact, where $r = r_T$ is the coordinate of the point contact.

The tunnel Hamiltonian H_T can be written on the standard form [4, 74, 75], with a hopping parameter κ determining the transfer properties of the junction. The interaction is assumed local, at the point contact,

$$\hat{H}_T = \hat{c}_L^\dagger(r_T,t)\hat{T}\hat{c}_R(r_T,t) + \text{h.c.}, \quad \hat{T} = \begin{pmatrix} \kappa & 0 \\ 0 & -\kappa^* \end{pmatrix}. \tag{2.5}$$

Here the hopping parameter is assumed energy independent, which is relevant for the atomic size point contact. A generalization to energy dependent scattering is discussed in Sec. 2.2, using scattering theory. The last term in Eq. (2.1) describes the Coulomb interaction. As long as we are only interested in large time scales compared to the inverse plasma frequency of the electrodes, the Coulomb interaction can be described by an effective capacitive interaction, depending on the charge difference between the two electrodes,

$$\hat{H}_Q = \frac{C}{2}V^2(t). \tag{2.6}$$

Here C is the usual capacitance defined by the geometric properties of the junction. Generally, we consider this capacitance as an individual branch coupled in parallel to the point contact, according to Fig. 2.1.

It is convenient to perform a gauge transformation, which removes the phase from the order parameter matrix $\hat{\Delta}$,

$$\hat{c}_L(r,t) \to e^{i\chi_L(r,t)\sigma_z/2}\hat{c}_L(r,t). \tag{2.7}$$

The corresponding procedure is performed also on the right electrode. The transformation, Eq. (2.7), yields a Hamiltonian with a real order parameter matrix in both electrodes,

$$\hat{H}_L = \int_{r\in L} d^3r\, \hat{c}_L^\dagger(r,t)\left[h_0\sigma_z + \Delta_L\sigma_x\right]\hat{c}_L(r,t), \tag{2.8}$$

where $h_0 = -\hbar^2\nabla^2/(2m) - \mu$. In this equation, the terms proportional to the superfluid velocity,

$$\vec{v}_s = \frac{\hbar}{2m}(\vec{\nabla}\chi - \frac{2e}{\hbar}\vec{A}), \tag{2.9}$$

have been omitted, since we consider electrodes which are large compared to the London penetration depth. Hence, the electrodes can be treated as bulk superconductors where the external magnetic field is screened completely and the current density is small.

The effect of the gauge transformation Eq. (2.7) on the tunnel Hamiltonian is the appearance of a dependence on the phase difference between the electrodes of the hopping parameter,

$$H_T = \hat{c}_L^\dagger(r_T,t)\hat{T}e^{i\phi(t)\sigma_z/2}\hat{c}_R(r_T,t) + \text{h.c.} \tag{2.10}$$

Current

The current through the point contact is given by the relation,

$$\hat{I}(t) = -e\frac{d}{dt}\hat{N}_L(t), \quad \hat{N}_L(t) = \int_{r\in L} d^3r\, c^\dagger(r,t)\sigma_z c(r,t), \tag{2.11}$$

The time derivative of the number operator $\hat{N}_L$ is conveniently calculated using the Heisenberg relation,

$$\hat{I} = \frac{ie}{\hbar}\left[\hat{N}_L(t), \hat{H}_T(t)\right] = \frac{ie}{\hbar}\hat{c}_L^\dagger(r_T,t)\hat{T}e^{i\phi(t)\sigma_z/2}\hat{c}_R(r_T,t). \tag{2.12}$$

Hence, the current operator can be written on the form,

$$\hat{I}(t) = \frac{2e}{\hbar}\frac{\partial}{\partial\phi}\hat{H}_T(t). \tag{2.13}$$

Since the Nambu vectors on both sides of the point contact are considered as bulk states, the current through the point contact depends only on the (fluctuating) phase difference and the transparency of the junction.

Functional integral approach

In order to calculate the effective Hamiltonian describing the slow quantum dynamics of the junction we employ a functional integral approach, similar to the technique used by Ambegaokar, Eckern and Schön [73, 76]. We can integrate out the degrees of

freedom of quasiparticle excitations in the electrodes and arrive at an effective action describing the slow, on the time scale $\hbar/\Delta$, non-dissipative dynamics of the phase difference and the Andreev states of the point contact.

The approach is based on the normalized partition function,

$$Z = \mathcal{N} \int D^2 c_L D^2 c_R D\phi \, e^{iS/\hbar}, \quad \mathcal{N}^{-1} = \int D^2 c_L D^2 c_R D\phi \, e^{iS_0/\hbar}, \tag{2.14}$$

where $S = S_p + S_C$ is the action for the point contact, S_p, including the electrodes, and the capacitive branch, S_C. The effective capacitance C can be adjusted by means of a shunt capacitor. In the functional formulation, $c_{L/R}(r,t)$ are complex Grassman fields, and the notation $D^2 c$ is short hand notation for the functional integration over the complex field $Dc^\dagger Dc$. The normalization constant $\mathcal{N}$ is given by the partition function for the uncoupled electrodes, $S_0 = S(\kappa = 0)$. The actions for the point contact S_p and the capacitor S_C are straightforward to derive from the Hamiltonian Eq. (2.1),

$$S_p = S_L + S_R - \int dt \; H_T(\phi) \tag{2.15}$$

$$S_L = \int dt \int_{r\in L} d^3 r \; c^\dagger(r,t)\{i\hbar\frac{\partial}{\partial t} - h_0\sigma_z - \Delta\sigma_x\}c(r,t). \tag{2.16}$$

$$S_C = \int dt \left(\frac{\Phi_0}{2\pi}\right)^2 \frac{C}{2}\dot{\phi}^2. \tag{2.17}$$

For simplicity we consider the same magnitude of the order parameter in the two electrodes, $\Delta_L = \Delta_R = \Delta$.

SQUID geometry

The model described above concerns two superconducting electrodes, connected only by the point contact, but the same description can also be used if the two electrodes are connected to a ring, i.e. a SQUID-geometry, see Fig. 2.1. The main new feature is that the phase difference across the junction depends on the phase gradient in the electrode,

$$\int_{\text{electrode}} dl \cdot \vec{\nabla}\chi = \phi \; (\text{mod } 2\pi), \tag{2.18}$$

where the integration goes around the electrode (well within the electrode compared to the London penetration depth). Zero superfluid velocity in the electrode implies that $\vec{\nabla}\chi - (2e/\hbar)\vec{A} = 0$ (given by Eq. (2.9)). Accordingly, the phase difference is a function of the external flux,

$$\phi = (2\pi/\Phi_0)\Phi_t \; (\text{mod } 2\pi). \tag{2.19}$$

The total flux Φ_t consists of the external flux Φ_e and the flux, $\tilde{\Phi} = IL$, induced by the circulating current, where L is the geometric inductance,

$$\Phi_t = \Phi_e + \tilde{\Phi}. \tag{2.20}$$

Finally, if we consider the SQUID geometry, the energy of the induced flux yields an additional term in the action, S_I, which is given by

$$S_I = -\int dt\, \frac{E_L}{2}[\phi - \phi_e]^2, \tag{2.21}$$

where $E_L = (\Phi_0/2\pi)^2/L$ and $\phi_e = 2\pi\Phi_e/\Phi_0$.

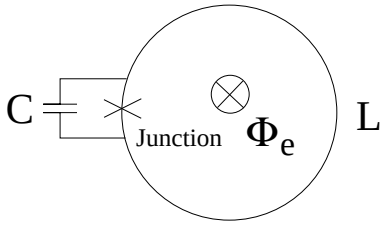

Figure 2.1: The effective electronic circuit of a junction in the SQUID-geometry, *i.e.* an rf-SQUID. L is the geometric inductance of the superconducting ring and C the effective capacitance of the junction.

Reduced Hamiltonian for the point contact

It is possible to simplify the action in Eq. (2.15) by integrating out the degrees of freedom of quasiparticle excitations outside the energy gap. This yields a crucial simplification of the problem, but requires that we only consider slow dynamics on the time scale $\hbar/\Delta$. The two Grassman fields $c_{L/R}$, for the left and the right electrode, in the interaction Hamiltonian H_T, Eq. (2.10), can be decoupled by introducing two new two-component Grassman fields $\theta(t)$ and $\eta(t)$ [77], following the Hubbard-Stratonovich procedure (see Appendix A),

$$e^{-\frac{i}{\hbar}\int dt\, H_T(\phi)} = \int D^2\eta D^2\theta\, e^{\frac{i}{\hbar}\int dt\left[\theta^\dagger \hat{T} e^{i\phi\sigma_z/2} c_L(r_T,t) + \eta^\dagger(\hat{T}e^{i\phi\sigma_z/2}c_R(r_T,t)+\theta) + \text{h.c.}\right]}. \tag{2.22}$$

After this decomposition, the functional integration over the Nambu field and the θ-field can be performed explicitly. We arrive at an effective action, which determines the slow dynamics of the phase difference ϕ and the Grassman field η [77], which describes the Andreev levels, as we will see later,

$$\begin{aligned} S_p[\phi,\eta] &= \int dt_1 dt_2\, \eta^\dagger(t_1) G^{-1}(t_1,t_2)\eta(t_2) \\ G^{-1}(t_1,t_2) &= g_0^{-1}(t_1-t_2) - \hat{T}(t_1) g_0(t_1-t_2)\hat{T}^{-1}(t_2). \end{aligned} \tag{2.23}$$

Here g_0 is the Green's function for the uncoupled electrodes ($\kappa = 0$), $g_0^{-1}(t_1 - t_2) = (i\hbar\partial_t - h_0\sigma_z - \Delta\sigma_x)\delta(t_1-t_2)\delta(r)$. The Fourier component, $g(\omega)$, is

$$g_0(\omega) = \frac{1}{\mathcal{V}}\sum_k \frac{1}{\hbar^2\omega^2 - E_k^2}\left(\hbar\omega + \epsilon_k\sigma_z + \Delta\sigma_x\right) \approx \frac{-i\pi N(0)}{\sqrt{\hbar^2\omega^2 - \Delta^2}}(\hbar\omega + \Delta\sigma_x), \tag{2.24}$$

where $\epsilon_k = \hbar^2 k^2/2m - \mu$, $E_k = \epsilon_k^2 + \Delta^2$, and $N(0)$ is the electron density of states at the Fermi level.

At small frequencies, $\hbar\omega \ll \Delta$, the Green's function in Eq. (2.24) is simplified further,

$$g_0(t_1 - t_2) = -\frac{\pi N(0)}{\Delta}(i\hbar\frac{d}{dt_1} + \Delta\sigma_x)\delta(t_1 - t_2). \tag{2.25}$$

Due to the low frequency approximation the full Green's function, Eq. (2.23), only depends on the time difference $t_1 - t_2$, which corresponds to a local effective action. It is convenient to include the constant factor in the front of $g_0(\omega)$, Eq. (2.25), in the field η. Then we arrive at the action [77]

$$S_p[\eta, \phi] = \int dt\, \eta^\dagger(t) \left[i\hbar\frac{d}{dt} + \hbar A\dot{\phi}\sigma_z - U_x\sigma_x - U_y\sigma_y \right] \eta(t), \tag{2.26}$$

where $A = \frac{1}{4}(1 - \sqrt{R})$, and

$$U_x = \Delta(\cos^2\frac{\phi}{2} + \sqrt{R}\sin^2\frac{\phi}{2}) \tag{2.27}$$

$$U_y = -2A\Delta\sin\phi. \tag{2.28}$$

The reflectivity of the junction is $R = 1 - D$, where D is defined by the equation [36],

$$D = \frac{N^2(0)\pi^2|\kappa|^2}{[1 + N^2(0)\pi^2|\kappa|^2]^2}. \tag{2.29}$$

It is convenient for later purposes to proceed to the Hamiltonian description. The conjugate momentum to η and the conjugate quasi charge to ϕ are

$$\begin{aligned} p_\eta &= \frac{\partial L}{\partial\dot{\eta}} = i\hbar\eta^\dagger \\ q_\phi &= \frac{2\pi}{\Phi_0}\frac{\partial L}{\partial\dot{\phi}} = \frac{\Phi_0}{2\pi}C\dot{\phi} + 2eA\sigma_z. \end{aligned}$$

Then we can use the Legendre transformation to get the Hamiltonian, $H = (\Phi_0/2\pi)q_\phi\dot{\phi} + p_\eta\dot{\eta} - L$. The variables ϕ and η are quantized by imposing the usual commutation relations, for Fermions and Bosons, respectively,

$$\begin{aligned} \{\eta_i, \eta_j^\dagger\} &= \delta_{ij} \\ [\phi, q_\phi] &= i2e. \end{aligned}$$

Finally, the reduced Hamiltonian takes the form [77],

$$\hat{H} = \frac{1}{2C}(q_\phi - 2eA\sigma_z)^2 + U_x(\phi)\sigma_x + U_y(\phi)\sigma_y, \tag{2.30}$$

where the quasi charge operator is $q_\phi = -i2e\partial_\phi$. This Hamiltonian describes the dynamics of the low energy levels and the phase difference in the system of the Josephson contact.

Note that the eigenvalues of the potential energy term in the Hamiltonian, Eq. (2.30), yields the bound Andreev level spectrum, $U_x^2 + U_y^2 = E_a^2$, where

$$E_a(\phi) = \Delta\sqrt{1 - D\sin^2\frac{\phi}{2}}. \tag{2.31}$$

It is straightforward to calculate the electrical current in the point contact using Eq. (2.13). Performing the gauge transformation, $\eta \to e^{iA\sigma_z\phi(t)}\eta$, which removes the σ_z-term from the kinetic part of the Hamiltonian in Eq. (2.30), we arrive at the current operator for the point contact,

$$\hat{I}(\phi) = I_a(\phi)[-\cos\frac{\phi}{2}\sigma_x + \sin\frac{\phi}{2}\sigma_y], \tag{2.32}$$

which has the eigenvalues $\pm I_a(\phi)$,

$$I_a(\phi) = \frac{eD\Delta}{\hbar}\sin\frac{\phi}{2}. \tag{2.33}$$

If we assume that the phase difference is time independent, it is straightforward to integrate out the η-field from Eq. (2.26). The resulting action is $S_p(\phi)/\hbar = \int d\omega\ \ln(\hbar^2\omega^2 - E_a^2(\phi))$. The average current, corresponding to Eq. (2.13), is then given by the equation,

$$I(\phi) = \frac{e\Delta}{\hbar}\frac{D\sin\phi}{2E_a(\phi)}, \tag{2.34}$$

which we recognize as the Josephson current in a point contact at zero temperature [27, 78].

Tunnel junctions

If the transparency of the junction is low, $D \ll 1$, then the dynamics of the Andreev states is on the time scale $\hbar/\Delta$. Hence, if we are interested in the slow dynamics, $\hbar\omega \ll \Delta$, it is relevant to integrate out also the field η, to get an effective action for the slow dynamics of the phase difference only.

Consider the point contact branch, the partition function of which is,

$$Z_p[\phi] = \mathrm{Det}[g_0^{-1}]\int D^2\eta\, e^{\frac{i}{\hbar}S_p[\eta,\phi]}, \tag{2.35}$$

where S_p and g_0 are given by Eq. (2.23) and Eq. (2.24), respectively. A straightforward evaluation of the η-integral yields,

$$\begin{aligned}
&\ln Z = \mathrm{Tr}\ \ln(1 - g_0\hat{T}g_0\hat{T}^{-1}) \\
&= -\mathrm{tr}\int dt_1 dt_2\, g_0(t_2 - t_1)\hat{T}(t_1)g_0(t_1 - t_2)\hat{T}^{-1}(t_2) + \mathcal{O}(D^2) \\
&= i\int dt_1 dt_2\ \left[a(t_1 - t_2)\cos\frac{\phi(t_1) - \phi(t_2)}{2} + b(t_1 - t_2)\cos\frac{\phi(t_1) + \phi(t_2)}{2}\right] \\
&+\mathcal{O}(D^2),
\end{aligned} \tag{2.36}$$

where we have used the approximation $D \approx 4N^2(0)\pi^2|\kappa|^2$, and where [73]

$$a(t) = -\frac{iD\hbar^2}{2}\int\frac{d\omega_1 d\omega_2}{(2\pi)^2}\frac{e^{-i(\omega_1-\omega_2)t}\omega_1\omega_2}{\sqrt{(\hbar^2\omega_1^2-\Delta^2)(\hbar^2\omega_2^2-\Delta^2)}},$$
$$b(t) = \frac{iD\Delta^2}{2}\int\frac{d\omega_1 d\omega_2}{(2\pi)^2}\frac{e^{-i(\omega_1-\omega_2)t}}{\sqrt{(\hbar^2\omega_1^2-\Delta^2)(\hbar^2\omega_2^2-\Delta^2)}}.$$

Assuming that the phase difference varies slowly on the time scale $\hbar/\Delta$, we can treat both the terms in Eq. (2.36) as local in time. Thus,

$$\cos\frac{\phi(t_1)-\phi(t_2)}{2} \approx 1-\frac{1}{8}\left(\frac{\partial\phi}{\partial t}\right)^2\tau^2, \quad \cos\frac{\phi(t_1)+\phi(t_2)}{2} \approx \cos\phi(t), \tag{2.37}$$

where $\tau = t_1 - t_2$ and $t = (t_1+t_2)/2$. We arrive at an action with a periodic potential term proportional to the Josephson energy, *i.e.* the "washboard potential", and a kinetic term, which yields a shift δC of the effective capacitance,

$$Z_p = e^{i\int dt\left[\left(\frac{\Phi_0}{2\pi}\right)^2\frac{\delta C}{2}\dot{\phi}^2+E_J\cos\phi\right]}, \tag{2.38}$$

where $E_J = \Phi_0 I_c/2\pi$ and the critical current for the single channel is $I_c = eD\Delta/2\hbar$. The shift of the effective capacitance is [73],

$$\delta C = -\frac{e^2}{\hbar}\int d\tau\,\tau^2 a(\tau). \tag{2.39}$$

The generalization to multi-mode tunnel junctions is straightforward, because of the separability of the conductance modes in short junctions; the total critical current can be presented as a sum of independent modes with transmission eigenvalues $D_I \ll 1$.

The least action solutions to the action $S = S_p + S_C$, where S_p is given by Eq. (2.38), are quite different depending of the ratio of E_C and E_J. If the charging energy dominates, $E_C \gg E_J$, there are no localized solutions but only Bloch states, which correspond to discrete quasi charge states on the electrodes ($\Delta q = 2e, 4e, 6e, ...$). The small Josephson coupling yields a hybridization of the quasi charge states and a Bloch-band structure, see [79]. In the opposite limit, $E_J \gg E_C$, the lowest bands are exponentially narrow $\Delta E \sim e^{-\sqrt{2E_J/E_C}}$ [80]. The lowest states of a local minimum in the periodic potential can then be approximated by the eigenstates to a harmonic oscillator.

2.2 SCATTERING THEORY

So far we have neglected all sorts of dissipation, in the junction and in the electrodes. The role of dissipation in ScS-junctions is a recent research field, and it has been investigated using both Green's function techniques [36, 81] and the scattering approach [34, 35]. When a voltage bias is applied to the junction, a nonequilibrium quasiparticle distribution develops in the contact area. In transparent junctions,

this effect is strong even for small voltages. The scattering approach is particularly useful for studying strong nonequilibrium and non-stationary effects in spatially non-homogeneous structures. Employing the Landauer philosophy [20] to ScS-structures, we assume that all inelastic quasiparticle processes occur in the electrodes, which are treated as equilibrium quasiparticle reservoirs. The scattering of quasiparticles in the normal region is assumed entirely dynamical. When studying the dissipative transport we will disregard effects of the fluctuating environment and consider the phase difference as a well defined classical variable. This corresponds to the regime $E_C \ll E_J$, when charging effects on the electrodes are not important.

The simplest assumption about the normal region of the junction is to consider it a conductor of the same material as the superconductor but with $\Delta = 0$. Moreover, we require that the width of the normal region varies slowly in space and that scattering only occurs at impurities, except of Andreev reflections at the NS interfaces. Hence, the normal region is considered as a non-superconducting waveguide for electrons and holes.

Consider one of the superconducting electrodes. We assume that the electrode is free of external fields and in equilibrium. Thus, it is described by the Hamiltonian Eq. (2.8). It is convenient to expand the Nambu operator $\hat{c}(r,t)$ in scattering states,

$$\hat{c}(r,t) = \sum_{\mu} c_\mu(r,t)\hat{a}_\mu, \tag{2.40}$$

where $c_\mu(r,t)$ are the scattering state wavefunctions and $\hat{a}_\mu^\dagger$ are the creation operators for the scattering states. The quantum number μ labels the quasiparticle state in a particular electrode. Since we consider reservoirs in equilibrium the incoming scattering states from different modes, and electrodes, are statistically independent, and the occupation number is given by the Fermi distribution function, $n_F = 1/(e^{E_\mu/k_BT}+1)$,

$$\langle \hat{a}_\mu^\dagger \hat{a}_\nu \rangle = \delta_{\mu\nu} n_F(E_\mu). \tag{2.41}$$

The scattering state consists of a linear combination of transmitted and reflected waves,

$$c_\mu(k) e^{ikr - iE_\mu t}, \tag{2.42}$$

where $c_\mu(k)$ satisfy the stationary BdG-equation [10],

$$[\epsilon_k \sigma_z + \Delta\sigma_x - E] c_\mu(k) = 0. \tag{2.43}$$

This equation describes the hybridization of electrons and holes in the vicinity of the energy gap, and gives the dispersion relation $k^\pm = \sqrt{2m(\mu \pm \xi)}/\hbar$, where

$$\xi = \begin{cases} \sqrt{E^2 - \Delta^2}, & |E| > \Delta \\ i\alpha\sqrt{\Delta^2 - E^2}, & |E| < \Delta \end{cases}, \tag{2.44}$$

where $\alpha = \mathrm{sign}\,(E)$. The wave vector $k^\pm$ is defined for electron-like $(+)$ and hole-like $(-)$ quasiparticles. The naming refers to the limit $\Delta \to 0$ when hole-like quasiparticles turn to holes and electron-like quasiparticles turn to electrons. The solutions to

Eq. (2.43) are,

$$c^{\pm}(E) = \frac{1}{\sqrt{2}}\min(1, \sqrt{\Delta/|E|})e^{\pm\gamma\sigma_z/2}c_0(E), \tag{2.45}$$

where $c_0(E) = (1, \alpha)$, and

$$e^{\gamma} = \frac{|E| + \xi}{\Delta}. \tag{2.46}$$

For $|E| > \Delta$ the solutions are free quasiparticles (plane waves) in the electrodes.

Now we have the necessary tools for calculating the electric current in the electrode. This is done by means of the operator for the current density,

$$\hat{j}(r,t) = \frac{e\hbar}{i2m}\hat{c}^{\dagger}(r,t)\vec{\nabla}\hat{c}(r,t) + \text{h.c.}, \tag{2.47}$$

which may be used either in the electrode or in the normal region. This expression is calculated for electron-like and hole-like quasiparticles, injected from the electrodes.

The NcS-interface

Apart from the bulk properties of the electrodes, we are also interested in the boundaries between the normal and the superconducting regions, and in the Andreev reflection in particular. We consider a single channel SN interface, with perfect contact between the superconducting and the normal reservoir. The scattering at the interface is conveniently calculated following the BTK approach [21], by means of matching the solutions, Eq. (2.45), in the normal and the superconducting regions. An important consequence of the energy gap is that electrons can be reflected back as holes, and vice versa, at the interface. The amplitude for this Andreev reflection is given by the equation,

$$r_a = \alpha e^{-\gamma(E)}. \tag{2.48}$$

Hence, the probability for Andreev reflection is unity in the gap, whereas it decays rapidly outside the energy gap, $|r_a|^2 \sim \Delta^2/|E + \xi|^2$. Conservation of charge implies that two electron charges must have been transferred to the superconducting region during the Andreev reflection: a Cooper pair has been added to the condensate. The emission of a Cooper-pair from the superconductor corresponds to the reversed process: a hole is Andreev reflected as an electron.

It should be noted that the expression, Eq. (2.48), is not entirely correct. Since the wave vectors in the superconducting and normal regions are not equal, there will always be a small amount of normal reflection. However, this effect is small, of the order of Δ/μ, and may be neglected if $\Delta \ll \mu$. The situation is obviously different if the contact between the two regions is not perfect. An insulating barrier at the interface will decrease the probability for Andreev reflections and instead increase the probability for normal reflections. This reduction of Andreev reflection is a well-known experimental problem, since transparent NS interfaces are difficult to create.

The wave function of a scattering state involving an Andreev reflection within the energy gap has an exponentially decaying tail in the superconducting electrode. An expansion of $k^{\pm}$ in the parameter $\Delta \ll \mu$ yields,

$$k^{\pm} = k_F \pm \xi k_F/\mu + \mathcal{O}(\xi^2/\mu^2), \tag{2.49}$$

where $k_F = \sqrt{2m\mu}/\hbar$ is the Fermi wave vector, and ξ is purely imaginary if $|E| < \Delta$. Hence, the wave function decays on the length scale $\xi_0 = \hbar v_F/\Delta$ in the superconductor.

Finally, we notice that Andreev reflections provide the only mechanism of current transport in the energy gap. This simple effect stands behind most of the phenomena studied in this thesis.

Transfer matrix formalism

It is convenient to introduce a transfer matrix formulation of the scattering in the normal region. This technique is convenient for analytical studies of multiple Andreev reflections, and it is used to large extent in Paper III; but it is also useful for calculating the equilibrium current in SNS junctions.

The SNS junction is modeled by a single channel normal wire in perfect contact with the superconducting electrodes at both sides, see Fig. 2.2. The interfaces of the two electrodes are located at $x = -L_1$ and $x = L_2$, where x is the coordinate along the normal wire, and there is an impurity in the junction, at $x = 0$. A detailed analysis of this particular SNS junction can be found in Ref. [29].

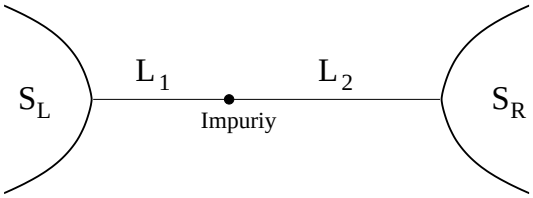

Figure 2.2: Schematic figure of the simplified quantum SNS junction with one impurity. The length of the normal region is $L = L_1 + L_2$.

We use a vector notation for the scattering amplitudes for waves propagating in both directions in the normal region, $a(E) = ((c_k^+)_1, (c_{-k}^+)_1)$, for electrons and $b(E) = ((c_k^-)_2, (c_{-k}^-)_2)$ for holes.

The regions between the impurity and the electrodes are assumed to be ballistic, which corresponds to the transfer matrix (from right to left),

$$T_{L_i}^{\pm} = e^{-ik^{\pm}L_i\sigma_z}. \tag{2.50}$$

The impurity is considered as an elastic point scatterer, whose transparency is independent of energy on the scale $\Delta \ll \mu$. It is described by a unitary scattering matrix,

which relates incoming and outgoing waves at both sides of the impurity. For electrons we can write,

$$\begin{pmatrix} a_2(0-) \\ a_1(0+) \end{pmatrix} = S \begin{pmatrix} a_1(0-) \\ a_2(0+) \end{pmatrix}, \quad S = \begin{pmatrix} r & d^* \\ d & -r^* \end{pmatrix}. \tag{2.51}$$

We can use the Hermitian conjugate of same scattering matrix for holes. The elements of the scattering matrix S determine the reflectivity of the impurity, $R = |r|^2$, and the transparency, $D = 1 - R = |d|^2$. The corresponding transfer matrix T_r has the form,

$$T_r = \frac{1}{d} \begin{pmatrix} 1 & -r \\ -r^* & 1 \end{pmatrix}, \tag{2.52}$$

and the equations for electrons and holes are the same,

$$a(0-) = T_r a(0+), \;\; b(0-) = T_r b(0+). \tag{2.53}$$

The scattering approach we consider here can be generalized for multi-terminal junctions, by increasing the dimensions of the scattering matrix S. This technique was introduced by Büttiker in 1984 [82], and we use it in Papers I-III to consider probes attached to the normal region of the SNS junction.

Due to the gauge transformation in Eq. (2.7) of the Nambu operators in the superconducting electrodes we have to include also the dependence of the transfer matrix on the phase difference between the electrodes,

$$\begin{aligned} T_N^{\pm} &= T_s^{\pm} e^{\pm i\phi/2}, \\ T_s^{\pm} &= T_{L_1}^{\pm} T_r T_{L_2}^{\pm}. \end{aligned} \tag{2.54}$$

The situation is slightly different if the gauge transformation, Eq. (2.7), is not performed: then the Nambu field, and hence the amplitude for Andreev reflection Eq. (2.48), are phase dependent. The reflected hole "picks up" the phase of the superconductor. Obviously, the results for both approaches are the same.

The transfer matrix in Eq. (2.54) is generally energy dependent, with the exception of short junctions, $L \ll \xi_0$, where this energy dependence can be neglected.

It is convenient to express also the scattering at the NS interfaces as a transfer matrix, which relates electrons and holes in the normal region. We use the Andreev approximation and neglect terms proportional to Δ/μ, just as in Eq. (2.48),

$$a(-L_1) = Ub(-L_1) + \delta_{1j} Y_\sigma$$

$$b(L_2) = Ua(L_2) + \delta_{2j} Y_\sigma \tag{2.55}$$

$$U = \mathrm{sign}\,(E)\, e^{-\gamma\sigma_z}, \tag{2.56}$$

$$Y_\sigma = \frac{\sqrt{2}\xi}{\sqrt{|E|}} e^{-\gamma\sigma_z/2} \begin{pmatrix} \delta_{1\sigma} \\ \delta_{-1\sigma} \end{pmatrix}, \tag{2.57}$$

where $\sigma = \pm 1$ and $j = 1, 2$ denote the type of quasiparticle and the electrode from which the quasiparticle is injected, respectively. The source term refers to the electron-like and hole-like quasiparticles, Note that the matrix in Eq. (2.56) obeys the standard transfer matrix equation, $U\sigma_z U^\dagger = \sigma_z$, only in the energy gap. Outside the gap there is a finite leakage to the superconducting electrode.

Andreev states in SNS junctions

The spectrum of the Andreev levels in a short SNS junction was derived in Sec. 2.1 and given by Eq. (2.31). Now we proceed and calculate the spectrum for junctions with finite length.

Inside the energy gap, $|E| < \Delta$, we can treat the SN interface as an ideal Andreev mirror, which turns electrons into holes and vice versa. The equations for the interface read,

$$a(-L_1) = Ub(-L_1), \quad b(L_2) = Ua(L_2), \quad U = \mathrm{sign}\,(E)\, e^{-\gamma\sigma_z}, \quad |E| < \Delta. \tag{2.58}$$

Combining these equations with the transfer matrix in Eq. (2.54) we can write an equation for the energy spectrum of the bound states,

$$a(-L_1) = Ue^{i\phi/2}T_s^- Ue^{i\phi/2}(T_s^+)^{-1}a(-L_1). \tag{2.59}$$

The solvability condition for this equation yields the equations for the spectrum,

$$\begin{aligned} \theta &= 2i\gamma - \beta_1 - \beta_2, \\ \cos\theta &= R\cos(\beta_1 - \beta_2) + D\cos\phi, \end{aligned} \tag{2.60}$$

where $\beta_i = 2EL_i/\hbar v_F$, and γ is given by Eq. (2.46). It follows from Eq. (2.60) that the number of Andreev levels depends on the total length of the junction. Fig. 2.3 shows a few examples, of which the simplest is for the short junction. If the length of the junction is much smaller than the superconducting coherence length, $L \ll \xi_0 = \hbar v_F/\Delta$, there are only two Andreev levels in the gap and the equations (2.60) reduce to the spectrum given by Eq. (2.31).

The Josephson current in the SNS junction consist of a contribution from the populated Andreev states and a contribution from continuum states [29],

$$I = \frac{2e}{\hbar}\sum_n \frac{\partial E_n(\phi)}{\partial\phi}\tanh\frac{E}{2k_BT} + I_{\mathrm{cont}}, \tag{2.61}$$

where the sum is over all Andreev levels under the Fermi level, $E_n < 0$, and I_{cont} is the current contribution from the continuum. The continuum contribution is straightforward to calculate using scattering theory and the current formula, Eq. (2.47), while the contribution from the bound states [28, 83] can be obtained by applying Eq. (2.13) to the Hamiltonian of the bound Andreev states.

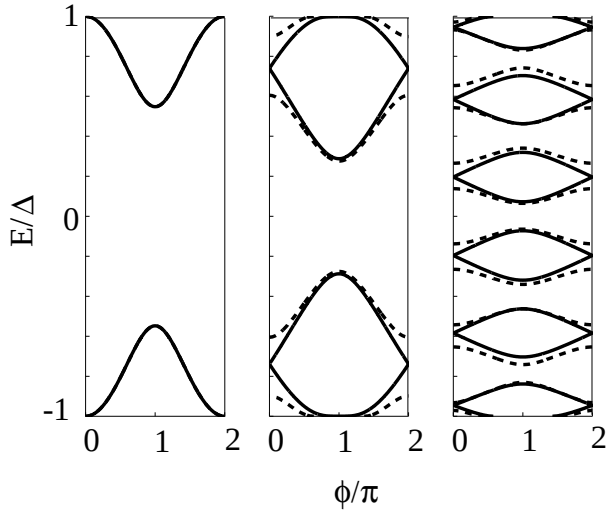

Figure 2.3: The Andreev levels as a function of the phase difference ϕ for different lengths; $L = 0$ (left), $L \sim \xi_0$ (middle) and $L \gg \xi_0$ (right). Solid lines show the spectrum for a symmetric junction, $L_1 = L_2$, and dashed lines shows the effect of asymmetry.

Multiple Andreev reflections

In this subsection we discuss the dissipative current which is produced by a constant voltage bias V applied to an SNS junction. This voltage bias yields a time dependent phase difference according to the Josephson relation, Eq. (2.4),

$$\phi(t) = \phi_{d0} + \frac{2e}{\hbar} Vt. \tag{2.62}$$

Historically, this problem was solved for ScS-junctions using various techniques during the period 1987-1995, see Refs. [33–37].

The scattering approach to voltage biased junctions is complicated, yet rather intuitive. A detailed derivation is presented in Paper III, where we use the technique to calculate the current-voltage characteristics for the SNS interferometer. I will not re-derive any equations here, but rather try to explain the theory quantitatively.

The time dependence of the phase difference ϕ appears in the scattering approach as a time dependence of the transfer matrix across the normal region, Eq. (2.54). This time dependence corresponds to an energy gain eV each time an electron travels from the left to the right border of the normal region, and correspondingly, the same energy gain for a hole traveling in the opposite direction. The result of this inelastic transport in the normal region, combined with the multiple Andreev reflections inside the energy gap, is that an incoming quasiparticle, with energy E, is scattered to sidebands at the energies $E_n = E + neV$, $n = 0, \pm 1, \pm 2, ...$ Note that these sidebands exist within the energy gap as well as outside.

The scattering states are straightforward to calculate using the transfer matrix technique described in the previous subsection. The problem is rewritten as series of re-

currences for the scattering amplitudes of different side bands (see Paper III). These recurrences are then solved with zero boundary conditions at plus and minus infinity in energy space.

The electric current is calculated by applying Eq. (2.47) to the scattering amplitudes in the normal region. The current is generally time dependent (the ac-Josephson effect), but we only consider the dc-part of the current. In order to provide a more transparent picture of the current transport we chose to expand the expression for the current in the *partial currents* J_n, involving $n-1$ Andreev reflections. In this way the current can be written as

$$I = \frac{e}{h} \sum_{j,n,\sigma} \int_{-\infty}^{-\Delta} dE [J_{n,j}(E) - J_{-n,j}(E)] \tanh \frac{E}{2k_B T}. \tag{2.63}$$

The current $J_{n,j}(E)$ is the current which is produced by injection of electron-like and hole-like quasiparticles from the electrode j, at energy E, and scattering to the n:th sideband, $E_n = E + neV$, see Fig. 2.4. Correspondingly, $J_{-n,j}$ is the current of the n-particle scattering process from E to $E_{-n} = E - neV$. Note that the $n-1$ Andreev reflections imply that the n-particle scattering process corresponds to the co-transfer of n electrons across the junctions.

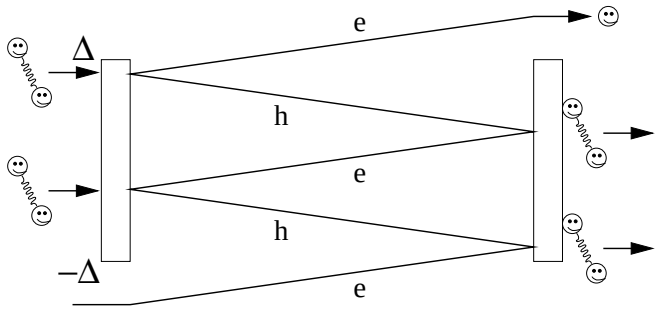

Figure 2.4: Diagrammatic picture of the 5-particle scattering process. This process can be viewed as the co-transfer of two Cooper-pairs and the electron through the junction.

The expression for the current, Eq. (2.63), can be further simplified using the detailed balance equation [84, 85],

$$J_{n,j}(E) = J_{-n,k}(E_n), \quad \begin{cases} k = j, & n \quad \text{even} \\ k \neq j, & n \quad \text{odd} \end{cases} \tag{2.64}$$

where $j \in \{1, 2\}$. The index k labels the electrode in which the n-particle scattering process, $J_{n,j}(E)$, ends. The identity, Eq. (2.64), is not obvious and has to be proved for every kind of junctions, which requires some algebraic excursions. However, it is valid for SNS junctions [84] and short SNS interferometers (see Paper III). An important consequence of the identity Eq. (2.64) is that only scattering processes which result in real excitations contribute to the current. All other processes cancel out each other.

Hence, at zero temperature only processes from the Fermi sea, at $E < -\Delta$, to empty states above the gap, $E > \Delta$, contribute to the current.

We can write the expression for the current, neglecting the contribution from thermal excitations, on the form

$$I = \sum_{n,j} I_{n,j} \tag{2.65}$$

$$I_{n,j}(E) = \frac{e}{h} \int_{\Delta - neV}^{-\Delta} dE \, J_{n,j} \tanh \frac{E}{2k_B T}, \tag{2.66}$$

where $I_{n,j}$ is the *n-particle current*, referring to the co-transfer of n electron charges.

Although the current voltage characteristics of SNS junctions are generally complicated and nonlinear, some important properties of the n-particle current, $I_{n,j}$, should be mentioned: the n-particle current is zero for $|V| < 2\Delta/n$, and the high order currents, $n > 2$, are suppressed at voltages, $(n-2)eV > 2\Delta$, due to the decaying probability of Andreev reflection outside the gap. Finally, if the n-particle scattering process is non-resonant, the amplitude of the corresponding n-particle current is proportional to D^n, where D is the transparency of the normal region.

CHAPTER 3

ANDREEV LEVEL INTERFEROMETRY

3.1 THE NS-INTERFEROMETER; PAPER I

An important aspect of Andreev reflection is that the phase of the Andreev reflection is shifted with the phase of the superconductor. This mechanism stands behind the Josephson effect in SNS junctions [13]. Spivak and Khemel'nitskii [86] showed that this effect also implies the possibility of interference of Andreev reflected particles from different regions of a superconductor with different phase. The NS-interferometer was proposed in 1991 by Nakano and Takayanagi [47,48]. They considered a Y-shaped normally conducting waveguide connected to two equipotential superconducting electrodes, but with different phase, and calculated the phase dependent conductance of the device. A similar geometry was investigated in 1993 by Hekking and Nazarov [49]. The first experiments with NS interferometers, showing phase dependent conductance oscillations, where presented in 1995 [50, 51]. For a review on more recent experiments, most of which are performed with diffusive junctions, see Ref. [87].

We consider the setup shown in Fig. 3.1, where the coupling of the NS-interferometer to the normal injection electrode is weak. In addition to the interference effect, this setup also exhibits strong effects due to quasibound Andreev states. Accordingly, the device may be useful for spectroscopy on Andreev levels.

We use the scattering approach to calculate scattering states for injection from

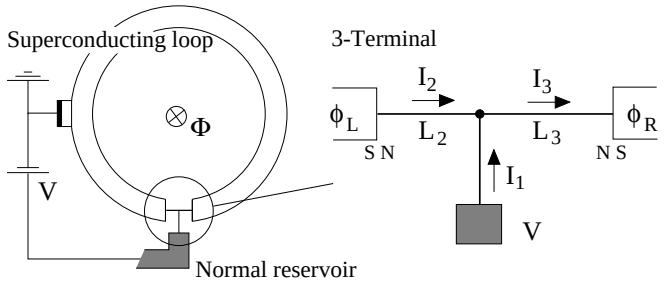

Figure 3.1: Schematic layout of the three terminal device, which is a phase biased, quantum SNS junction where the normal region is connected to a voltage biased normal reservoir. [Fig 1. in Paper I].

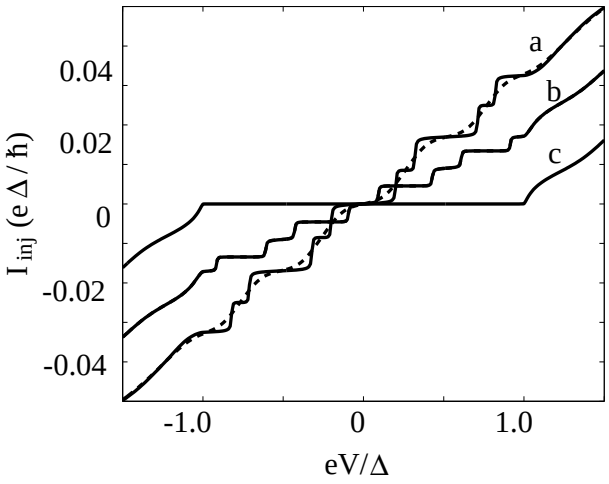

Figure 3.2: The injection current in the three terminal device as a function of the voltage for (a) $\phi =_d \pi/4$, (b) $\phi = 3\pi/4$ and (c) $\phi = \pi$. Zero temperature (solid lines) and $T = 0.05\Delta$ (dashed line) with $D = 0.8$, $L = 10\xi_0$ and $\epsilon = 0.05$. Note the vanishing subgap current at $\phi = \pi$. [Fig 14. in Paper I]

the normal reservoir and the two superconducting reservoirs. Knowing the scattering states, the current can be calculated by means of the formula Eq. (2.47). The scattering in the normal region is modeled with a Y-shaped single mode quantum wire and the scattering between the three leads is determined by a unitary scattering matrix [82],

$$S = \begin{pmatrix} \sqrt{1-2\epsilon} & \sqrt{\epsilon} & \sqrt{\epsilon} \\ \sqrt{\epsilon} & r & d \\ \sqrt{\epsilon} & d & r \end{pmatrix}, \tag{3.1}$$

where ϵ, $0 \leq \epsilon < 0.5$, is the coupling parameter to the normal reservoir. It is assumed that injected particles split equally into the two arms of the NS interferometer. Note that the limit $\epsilon \to 0$ yields the same junction as was discussed in Sec. 2.2; a quantum SNS junction with the length $L = L_1 + L_2$ and one impurity with transparency $D = |d|^2$. The Andreev spectrum for this particular junction is given by Eq. (2.60), see also Fig. 2.3. For arbitrary coupling ϵ we have the unitarity condition $R + D = 1 - \epsilon$. The two superconducting electrodes can have a finite phase difference, ϕ, and a voltage V is applied to the normal reservoir.

The current-voltage characteristics for the NS-interferometer is shown in Fig. 3.2. In the sugbap voltage region, $V < \Delta/e$, the current structures are staircase-like, where the steps are most pronounced for small coupling $\epsilon \ll 1$. For higher voltages the current-voltage characteristics are linear and the conductance is given by the normal conductance. The positions and the amplitudes of all structures in the subgap voltage region are phase dependent, the most significant effect being the vanishing subgap current at $\phi = \pi$.

The structures and the phase dependence of the subgap current is the result of two mechanisms: resonant Andreev transport and interference. The staircase-like structure

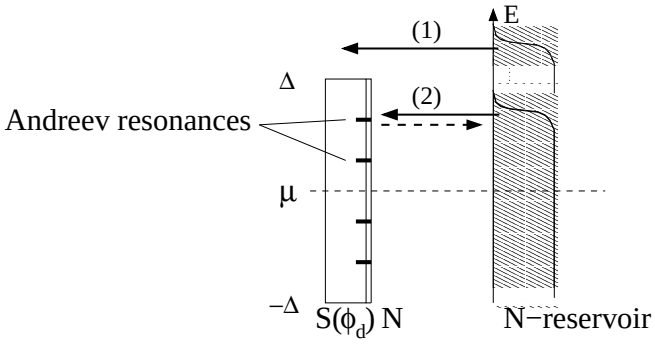

Figure 3.3: Schematic picture of the NS interferometer as an effective phase dependent $NS(\phi)$ interface. The current is carried by single particle transport (1) and Andreev transport (2). The Andreev transport is affected both by quasibound Andreev states, causing the current steps at $eV = E_{a,n}$, and interference, which kills the subgap current at $\phi = \pi$.

in the subgap voltage region is due to resonant Andreev reflection, which yields steps at voltages corresponding to the bound states, see Fig. 3.3. Hence, the positions of the current steps resembles the Andreev spectrum of the decoupled junction ($\epsilon = 0$), see Fig. 2.3. The overall amplitude of the current structures in the subgap region oscillates with phase due to the interference of Andreev reflected particles, see Fig. 3.2. For a symmetric junction, $L_1 = L_2$, the subgap current vanishes at $\phi = \pi \pmod{2\pi}$, while the single particle current remains and gives the linear current-voltage characteristics for large voltages, $V \gg \Delta/e$.

Nonequilibrium Josephson effect

There is another interesting aspect of the NS interferometer: modification of the Josephson current through the interferometer due to nonequilibrium, introduced in the normal region by the injection current. It is appealing to explore this possibility to control the Josephson current in SNS junctions by means of normal injection. The subject is interesting both from a fundamental physical point of view but also due to the possibility to construct superconducting transistors. It has been shown experimentally that the Josephson current can be suppressed by injection from a normal reservoir, both in ballistic [46] and diffusive [88, 89] SNS-junctions. Furthermore, it is demonstrated in reference [90] that the Josephson current may even be reversed. The first theoretical work on nonequilibrium Josephson effect by normal injection was presented by van Wees *et al.* in 1991 [91], considering both the broadening of the Andreev states due to the coupling to the normal reservoir and nonequilibrium population. It has further been demonstrated by Wendin and Shumeiko [56] that the nonequilibrium population of Andreev states may reveal considerable currents in both directions, large enough to reverse the Josephson current [57, 92]. This effect can be explained by considering the currents through individual Andreev states in long junctions (compare with Fig. 2.3 and Eq. (2.61)), which carry current in altering directions and tend to cancel out each other. Hence, the effect of one extra level, being populated by external injection, is

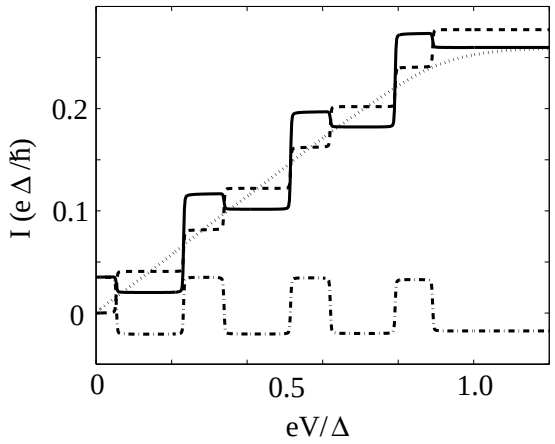

Figure 3.4: The total current $I_{eq}+I_r+I_a$ (solid line), I_r+I_{eq} (dash-dotted) and the anomalous current I_a (dashed) as a function of the voltage at zero temperature. $D = 0.8$, $\phi = 3\pi/4$, $\epsilon = 0.01$ and $L = 20\xi_0$. The total current for temperatures $kT \gg \hbar v_F/L$ is shown with a dotted line. [Fig. 9 in Paper I]

significant, and the current carried by this level might even overcompensate the equilibrium current and yield a negative supercurrent. What was further demonstrated by Samuelsson *et al.* [57] is that the current in the three terminal device (see Fig. 3.1) is not only changed by nonequilibrium population of Andreev states; the injection also affects the form of the wavefunction of the Andreev states. It was shown that injection of electrons and holes from the normal reservoir changes the Andreev states in different ways. This asymmetry produces an additional contribution to the current from each level, which has the same sign for all Andreev levels. This *anomalous* Josephson current is length independent and can be as large as the critical current in a short junction, for a voltage $V \sim \Delta/e$, applied to the normal reservoir.

Fig. 3.4 shows the Josephson current in a SNS junction with the length $L = 20\xi_0$ as a function of the voltage V applied to the normal reservoir. The coupling to the normal reservoir is small, $\epsilon \ll 1$, in order to sharpen the structures and to suppress the injection current. The current-voltage characteristic is staircase-like, with current steps at the resonant energies, $eV = E_{a,n}$. For voltages above the gap $eV > \Delta$ the current levels out and remains rather constant. If the length of the junction is increased the number of current steps in the subgap region increase, while the amplitude at large voltages remains rather length independent.

We distinguish two contributions to the nonequilibrium current: the *regular* current, which is the sum of the currents caused by injection of electrons and holes from the normal reservoir, $I_r = I_e + I_h$, and the *anomalous* current, which is proportional to the difference, $I_a = I_e - I_h$. Provided a weak coupling to the normal reservoir, $\epsilon \ll 1$, when the injected current from the normal reservoir can be neglected, the total nonequilibrium Josephson current is given by $I_T = I_{eq} + I_a + I_r$, where I_{eq} is the equilibrium Josephson current. The regular current jumps in altering direction every time

a new Andreev state is populated, and the IV-characteristic is hence oscillating in the subgap voltage region, see Fig. 3.4. The IV-characteristics of the anomalous current is staircase-like; the current steps when new Andreev states are populated have all the same sign. Hence, the anomalous current gets more significant when the length of the SNS junction is increased, since the equilibrium current dies exponentially with the length, due to the cancellation of the Andreev state currents, when the anomalous current remains rather constant. As a consequence, the three-terminal device may function as a transistor, where the anomalous current is turned on by increasing the voltage on the injection electrode from zero to Δ [93]. The gain of the transistor can be large if the coupling to the normal reservoir is weak $\epsilon \ll 1$. The amplitude of the regular current is of the order D, while the amplitude of the anomalous current is $\sqrt{RD}$, the sign of which also depends on the phase of the scatterer.

Interface barriers

Any realistic junction will have a finite probability for normal reflection at the NS-interfaces. Hence, it is relevant to consider the SNS-junction and the three-terminal device with interface barriers.

If we for a moment restrict ourselves to the case $\epsilon = 0$, we can use the technique described in Sec. 2.2 to calculate the bound state spectrum. It is convenient to look at the case $R = 0$, *i.e.* a SINIS junction [94], where we can write the equation for the Andreev levels on the form,

$$D_b^2 \cos\phi + 2R_b \cos\beta - \cos(2i\gamma - \beta) - R_b^2 \cos(2i\gamma + \beta) \\ -4R_b \sin^2 i\gamma \cos\beta_0 = 0,$$

where $\beta_0 = 2E_{BW}^{e,h}/(\hbar v_F/L)$, the quantity $E_{BW}^{e,h} = \pm 2\mu(1 - \pi(n - \mathrm{Arg}(r_d))/k_F L)$, $n = 0, \pm 1, \pm 2, ...$, denotes the energies of the Breit-Wiegner resonances in the junction, for electrons $(+)$ and holes $(-)$, and R_b and $D_b = 1 - R_b$ denote the reflectivity and the transparency, respectively, of the (symmetric) interface barriers. The case with nonzero R does not alter the picture in any crucial way.

Fig. 3.5 shows the length dependence of the Andreev spectrum in the presence of interface barriers. For transparent interface barriers there is small effect on the Andreev spectrum and hence also on the current. However, as the interface barriers are increased the bound states are pinned to the Breit-Wiegner resonances. Accordingly there is a fast length dependence of the current, with periodic resonant peaks on the length scale of the Fermi wavelength, see Fig. 3.5. The effect on the anomalous current is similar to the regular current with a strong length dependence on the scale λ_F. In resonance, the amplitude of the anomalous current is of the order, $I_a \sim D_b\sqrt{RD}$, and out of resonance, $I_a \sim D_b^2\sqrt{RD}$.

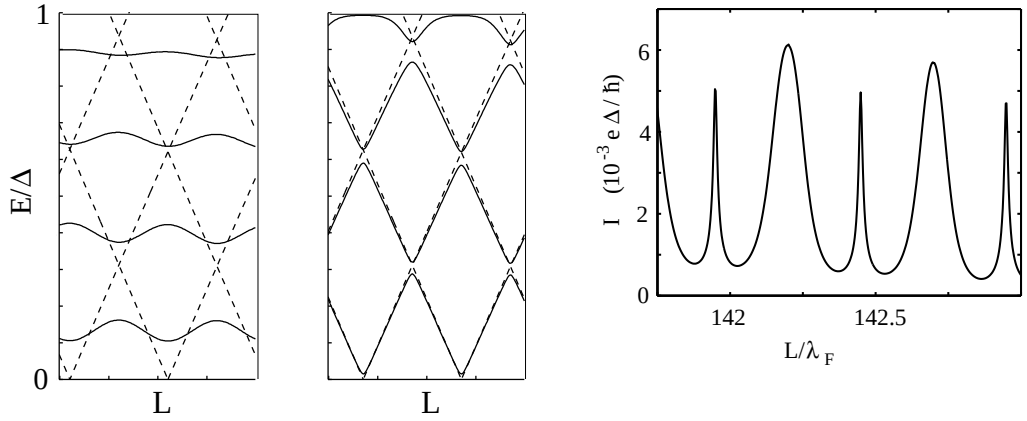

Figure 3.5: Left: The Andreev levels (solid) and the normal electron and hole resonances (dotted) as functions of the length L of the junction. We consider a junction with four Andreev states in (a) the weak resonance limit $R_b \ll 1$, (b) the strong resonance limit $R_b \sim 1$. Right: Current peaks due to Breit-Wiegner resonances in a three terminal device junction with interface barriers. The plot shows a short segment of the length dependence of the current. The junction is long $L \gg \xi_0$, with $R_b = 0.9$, $\epsilon = 0.01$ and $\phi = \pi/2$. [Fig. 12 (left) and Fig. 13 (right) in Paper I]

3.2 SNS-INTERFEROMETERS; PAPERS II AND III

In 1997 Kutchinsky *et al.* found phase dependent current structures in the subgap region of the IV-characteristics of their SNS-interferometer [52–55]. The effect was small, a natural consequence of the diffusive nature of the normal region, but nevertheless clear and reproducible.

Encouraged by these experiments, we consider a simplified SNS-interferometer where the normal region is an Y-shaped single channel wave guide. The design is similar to the three terminal device which was discussed in the previous section, but in this case the injection electrode is also superconducting. Since we apply a voltage to the injection electrode S_3, MAR is the mechanism of current transport through the interferometer. Moreover, since the two electrodes, S_1 and S_2, can have a finite phase difference, we expect phase dependent MAR and effects of quasi bound Andreev states.

We use a similar scattering matrix as for the NS-interferometer, Eq. (3.1), assuming that injected particles scatter in both directions in the SNS junction with equal probability. Note however that the numbering of the leads now is changed to be in line with the formalism in Paper III,

$$S = \begin{pmatrix} r & d & \sqrt{T} \\ d & r & \sqrt{T} \\ \sqrt{T} & \sqrt{T} & r_0 \end{pmatrix}, \tag{3.2}$$

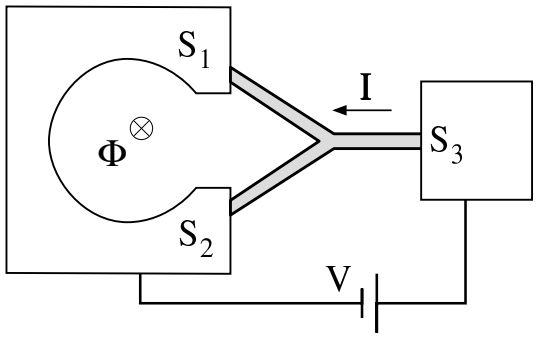

Figure 3.6: Schematic picture of the SNS interferometer, where the normal region is a Y-shaped waveguide. [Fig. 1 in Paper III]

where T is the coupling parameter, and the scattering matrix obeys the unitarity conditions, $R + D = 1 - T$, and $1 = |r_0|^2 + 2T$.

In order to employ the MAR approach, discussed on page 22, we perform a unitary transformation of the scattering amplitudes in the normal region, which allows us to treat the interferometer as an effective two terminal junction. The scattering in the normal region is then determined by an effective transfer matrix with transparency $2T$. The scattering at the *right* NS interface is usual Andreev reflection while the scattering at the *left* interface is given by the effective transfer matrix,

$$U_{\text{eff}}(\phi) = \frac{\text{sign}\,(E)}{\cos\frac{\phi}{2}} \left(e^{-\gamma\sigma_z} + \sigma_z(\sigma_x e^{i\theta\sigma_z} - 1)\frac{\Delta}{2\xi}\sin^2\frac{\phi}{2} \right), \tag{3.3}$$

where $\theta = \text{Arg}[(r-d)r_0]$. Here we have omitted the source term, for incoming electron-like and hole-like quasiparticles from the reservoir, which is however straightforward to derive in the same manner. The reflection consists of both Andreev- and normal reflection, depending on the phase difference, the probability of Andreev reflection of which is given by the matrix element $|(U_{\text{eff}})_{11}|^{-2} \sim \cos^2\frac{\phi}{2}$, which is indeed zero at $\phi = \pi$. The transfer matrix $U_{\text{eff}}(\phi)$ also contains information about the quasi-bound Andreev states in the interferometer.

Using the scattering approach to MAR we can then calculate the IV-characteristics of the SNS interferometer. Analytical solutions can be found in the weak coupling limit, $T \ll 1$, but for general transparency we rely on numerical simulations. We restrict the analysis to short interferometers, $L_i \ll \xi_0$ ($i = 1, 2, 3$), where the current structures become less complicated and easier to interpret.

Fig. 3.7 shows the typical IV-characteristics for a short SNS interferometer with low transparency $T \ll 1$. At zero phase difference we recognize the current-voltage characteristics of the quantum point contact [34, 35], with subharmonic gap structures. Increasing the phase difference, we find large current structures in the subgap region, with amplitudes proportional to the first power of the transparency T. We recognize two significant current peaks in the low voltage region, which both are related to the

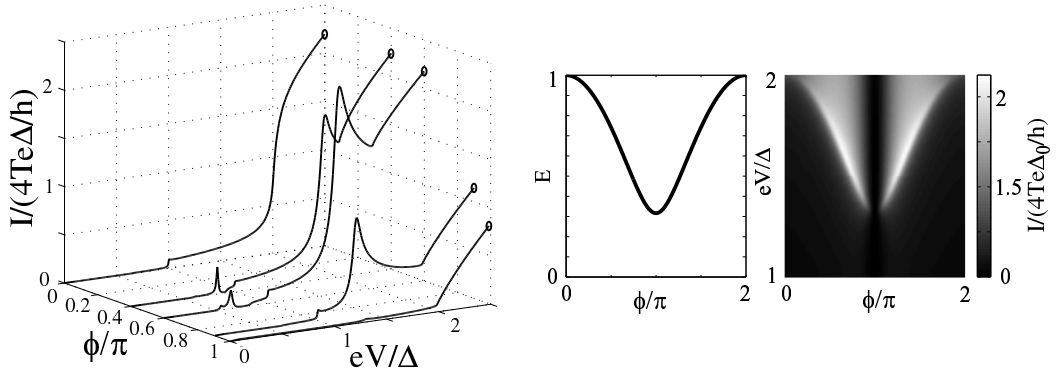

Figure 3.7: Left: Current voltage characteristics of the SNS-interferometer with $2T = 0.08$, $R = 0.1$ and $\phi = 0, 2\pi/5, 3\pi/5, 0.9\pi, 0.99\pi$. Right: the Andreev spectrum for $D = 0.9$, The current peak at $eV \approx \Delta + E_a$ follows the position of the Andreev level. [Fig. 7 (left) and Fig. 9 (right) in Paper III]

Andreev spectrum: at $eV \approx \Delta + E_a$ and at $eV \approx E_a$. Further we notice that the current structures disappear at $\phi = \pi$ in a way similar to the subgap current in the NS interferometer, Fig. 3.2.

For junctions with finite length, *e.g.* $L > \xi_0$, the current-voltage characteristic is different and generally more complicated, with a rich subgap structure of resonant peaks, due to the increased number of resonances. Nevertheless, it is still possible to attribute some of the current structures to the quasibound Andreev states in the junction. The phase dependence of these structures due to interference of Andreev reflected particles remains, being most pronounced if $L_1 = L_2$.

Another problem, which is not addressed in this thesis, is the nonequilibrium Josephson current in the SNS-interferometer. This is an interesting direction for future work on the SNS interferometer.

Resonance approximation

A perturbative analysis of the n-particle currents is possible if the coupling to the injection electrode is weak, $T \ll 1$. If we first consider the single particle current, *i.e.* quasiparticle tunneling, we find an expression in the weak-coupling limit that resembles the standard form of tunnel current,

$$I_1 = \frac{4eT}{h} \int_{\Delta - eV}^{\Delta} dE\, N_L(E) N_R(E + eV), \tag{3.4}$$

where $N(E)$ determines the effective superconducting density of states in the electrodes.

$$N_L(E) = \frac{|E|\sqrt{E^2 - \Delta^2}}{E^2 - E_a^2(\phi)}, \quad N_R = \frac{|E|}{\sqrt{E^2 - \Delta^2}}, \tag{3.5}$$

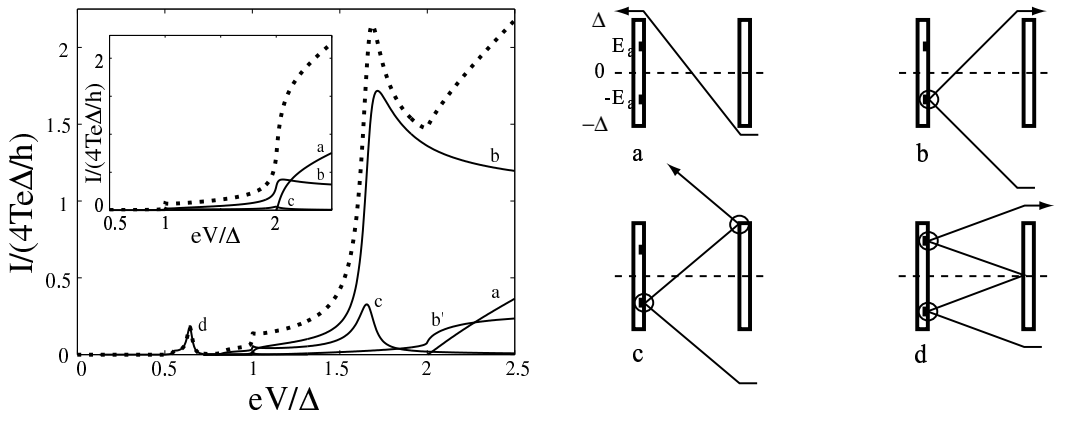

Figure 3.8: Left: The individual n-particle currents of the same interferometer as in Fig. 3.7, with $\phi = 3\pi/5$ and (inset) $\phi = 0$. The total current is dotted. The single particle current (a), the pair current from the right (b), the pair current from the left is non-resonant and small (b'), the 3-article current (c) and the 4-particle current (d). Right: Important diagrams of scattering processes, with the resonances shown as circles. [Fig. 5 (left) and Fig. 6 (right) in Paper III]

The form of $N_R(E)$ is well known from the BCS theory, but the effective density of states at the double-NS interface is phase dependent and the usual peaks at the gap edges vanish at nonzero phase difference. Instead, Andreev states develop in the gap, see Fig. 3.9. The result is a phase dependent onset of the single particle current at $V = 2\Delta/e$, see Fig. 3.8a.

The two-particle current is dominated by the two processes with one resonant Andreev reflection at the left SN interface, see Fig. 3.8b. The current from these resonances can be written on a Breit-Wiegner form,

$$I_2 = \frac{4e}{h}\int_{\Delta-2eV}^{\Delta} dE_1 \, \frac{\Gamma_+\Gamma_-}{(E_1 - E_a)^2 + (\Gamma_+ + \Gamma_-)^2/4}, \tag{3.6}$$

where the width of the resonance is given by

$$\Gamma_\pm = T D_\pm N_R(E_a \mp eV), \quad D_\pm = \frac{1}{2}\left[\sqrt{\Delta^2 - E_a^2} \pm \frac{\sqrt{DR}\Delta^2}{E_a}\sin^2\frac{\phi}{2}\right]. \tag{3.7}$$

The effective transparency of the Y-shaped normal region lies in the interval, $0 \leq TD_\pm \leq T\sqrt{D}$, and it is different for electrons and holes (incoming and Andreev reflected particles). Moreover, the interference due to the reflection by the double-NS interface appears as the factor $D_+D_- \sim \cos^2(\phi/2)$ and kills the two-particle current at $\phi = \pi$. Evaluation of the integral in Eq. (3.6) yields a resonant current, $I_2 = (4e/\hbar)\Gamma_+\Gamma_-/|\Gamma_+ + \Gamma_-|$, which is of the order T for $eV \geq \Delta + E_a$. The overshoot near $eV = \Delta + E_a$ appears due to the increased density of states near the gap in the right electrode, see Fig. 3.9.

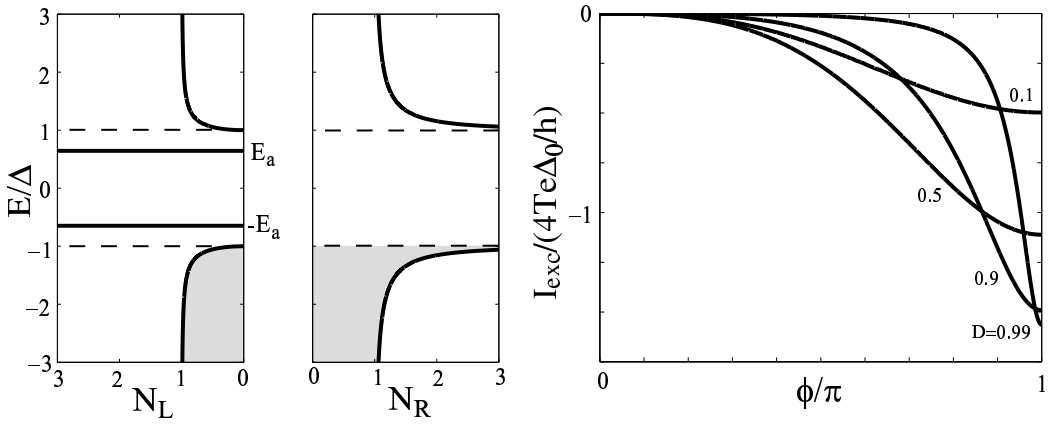

Figure 3.9: The effective density of states in the left and the right electrode for $D = 0.9$ and $\phi = 3\pi/5$. The shaded areas represent filled states at zero temperature.

The current peak at $eV \approx E_a$ emerges due to resonant 4-particle current, where two Andreev reflections at the left electrode occur at the resonant energies $E_1 = -E_a$ and $E_3 = E_a$, see Fig. 3.8d. Near the current peak, $e\delta V = eV - E_a \ll \Delta$, the 4-particle current is dominated by the double resonance and can be written as

$$I_4 = \frac{e}{h}\int_{-\infty}^{\infty} dE_2 \, \frac{\Gamma_0^2 \tilde{\Gamma}_-^2}{[E_2^2 - (e\delta V)^2 - \frac{1}{4}(\Gamma_0^2 + \tilde{\Gamma}_-^2)] + E_2^2 \tilde{\Gamma}_-^2}, \tag{3.8}$$

where

$$\Gamma_0 = TD_+, \quad \tilde{\Gamma}_- = TD_- N_R(2E_a). \tag{3.9}$$

The fully developed resonance yields a full-scale current structure, $\sim T$, which exists within the voltage interval, $\Delta/2 < eV < \Delta$, and the phase interval, $0 < \sin^2\phi < 3/4D$.

Finally, we will discuss the IV-characteristics for large voltages, $eV \gg \Delta$. We know from the work in Ref. [34–37] that the excess current in superconducting constrictions is of the order T^2. The situation in the SNS interferometer is different, for nonzero phase difference, mainly due to the interference effect in the junction. This interference effect suppresses the current at $\phi = \pi$ and yields a negative excess current of the order T.

We calculate this negative excess current in the weak coupling limit, neglecting terms of order T^2. The single particle current at high voltages consists of an Ohmic part and a negative phase dependent part,

$$I_1 = \frac{4Te^2V}{h} + I_{1,\mathrm{exc}}, \quad I_{1,\mathrm{exc}} = -\frac{eT\Delta\sqrt{D}}{h}|\sin(\phi/2)| + \mathcal{O}(T^2), \tag{3.10}$$

The current from Andreev transport, *i.e.* the two particle current given by Eq. (3.6), depends strongly on the phase difference and vanishes for $\phi = \pi$. Thus, although the

two particle current is resonant for nonzero phase difference it cannot compensate the reduced single particle current at $\phi = \pi$. The phase dependent current oscillations at large voltages are given by the non-Ohmic part of the single particle current, Eq. (3.10), plus the contribution from the resonant two particle current, Eq. (3.6),

$$I_{\rm exc} = -\frac{eT\Delta\sqrt{D}R}{h}\frac{|\sin(\phi/2)|^3}{E_a^2(\phi)} + \mathcal{O}(T^2). \tag{3.11}$$

This negative excess current at $\phi = \pi$ is of the order of the junction transparency T, which is unusual if we compare to two terminal ScS-junctions where the excess current is small $\sim T^2$ and positive. The excess current in Eq. (3.11) is plotted as a function of the phase difference in Fig. 3.9.

CHAPTER 4

SLOW DYNAMICS OF THE ANDREEV STATES

This chapter aims to give an insight into the slow dynamics of the Andreev states in a nearly transparent quantum point contact in a superconducting ring, and to explain the results discussed in Paper IV. Furthermore, the results in Paper IV are generalized to take into account the phase fluctuations, which are associated with the SQUID-geometry, using the results of Ref. [77].

4.1 THE ANDREEV LEVEL QUBIT; PAPER IV

Consider a nearly transparent, $R \ll 1$, quantum point contact in a non-hysteretic SQUID geometry, $E_L \gg \Delta$, where $E_L = (\Phi_0/2\pi)^2/L$. The setup is shown schematically in Fig. 2.1. The device is biased with a constant external flux $\Phi_e \approx \Phi_0/2$, when the Andreev levels are close to the Fermi level, $E_a(\phi_e) \approx \sqrt{R}\Delta \ll \Delta$. It has been shown experimentally that the transparency of a single channel point contact can be as good as $R \approx 0.01$ [45].

The Hamiltonian for the point contact and the superconducting ring is given by Eq. (2.30), including the potential term related to the superconducting ring, see Eq. (2.21),

$$\hat{H} = \frac{1}{2C}(q_\phi - 2eA\sigma_z)^2 + U_x(\phi)\sigma_x + U_y(\phi)\sigma_y + \frac{E_L}{2}(\phi - \phi_e)^2, \qquad (4.1)$$

where U_x and U_y are given by Eq. (2.27) and Eq. (2.28), respectively.

Using the gauge transformation, $\eta \to e^{iA\sigma_z(\phi(t)-\phi_e)}\eta$, we can separate the harmonic oscillator Hamiltonian, $H_{\rm h.o.}$, of the effective LC-circuit from the Hamiltonian, H_p, of the point contact,

$$\hat{H} = \hat{H}_p(\phi) + \hat{H}_{\rm h.o.}, \quad \hat{H}_{\rm h.o.} = \frac{q_\phi^2}{2C} + \frac{E_L}{2}(\phi - \phi_e)^2. \qquad (4.2)$$

Since we consider the non-hysteretic regime of the device $E_L \gg E_J \sim \Delta$ the amplitude of the zero point fluctuations of the induced flux are small, $1 \gg \tilde{\phi} = \phi - \phi_e$, and we can expand the Hamiltonian in $\tilde{\phi}$,

$$\hat{H}_p(\phi) = \hat{H}_a(\phi_e) + \frac{\partial \hat{H}}{\partial \phi}(\phi_e)\tilde{\phi}(t) + \mathcal{O}(\tilde{\phi}^2). \qquad (4.3)$$

Generally the same expansion can be used for small time dependent variations of the external flux, such as an applied rf-signal. The constant term, H_a, in Eq. (4.3) is the two-level Hamiltonian of the unperturbed Andreev levels, which we refer to as the Andreev state Hamiltonian. The linear response to fluctuations of the flux $\tilde{\phi}$ is given by the current operator, Eq. (2.32). We can write the Andreev state Hamiltonian, H_a, on a more convenient form, in the eigen basis of the current operator,

$$\hat{H}_a(\phi_e) = \Delta[\cos\frac{\phi_e}{2}\sigma_z + \sqrt{R}\sin\frac{\phi_e}{2}\sigma_x] \tag{4.4}$$

The current operator is hence diagonal,

$$\hat{I} = I_a(\phi_e)\sigma_z, \tag{4.5}$$

where $I_q(\phi_e) = (eD\Delta/\hbar)\sin(\phi/2)$.

The influence of the LC-circuit on the dynamics of the two-level system can be calculated analytically if the level splitting of the harmonic oscillator is large, $\hbar\omega_p \gg E_a(\phi_e)$, where $\hbar\omega_p = \sqrt{2E_C E_L}$ and $E_C = (2e)^2/2C$. In this case the two Andreev levels are well separated from higher energy levels, including the continuum of states outside the gap, $E_a \sim \sqrt{R}\Delta \ll \Delta$. Without any approximation, we can rewrite the full Hamiltonian as

$$\hat{H} = \hat{H}_a(\phi_e) + \frac{q_\phi^2}{2C} + \frac{E_L}{2}(\tilde{\phi} + \tilde{\phi}_0\sigma_z)^2, \tag{4.6}$$

where the displacement is, $\tilde{\phi}_0 = I_a\hbar/2eE_L$, and a constant energy term has been omitted. Thus, we have two identical but displaced harmonic oscillators, each having the energy spectrum $E_n = \hbar\omega_p(n+1/2)$ and the wave functions It is straightforward to show that there are no transitions between different states in a single well and that the inter-well transitions are proportional to $(\Delta\sqrt{R}/\hbar\omega_p)q_{nm}$, where q_{nm} is the matrix element between levels n and m in different oscillators. Thus, if $\hbar\omega_p \gg \Delta\sqrt{R}$, and $k_BT \ll 2E_a$, we can assume that only the ground states of the two oscillators are occupied. Under this assumption, it is straightforward to average over the plasma oscillations to get a Hamiltonian for the slow fluctuations between the average current states, having opposite directions in the ring. The resulting two-level Hamiltonian resembles the Andreev state Hamiltonian, but has renormalized non-diagonal terms [77],

$$\hat{H} = \Delta[\cos\frac{\phi_e}{2}\sigma_z + \sqrt{R}q_{00}\sin\frac{\phi_e}{2}\sigma_x], \tag{4.7}$$

where $q_{00} = \int d\tilde{\phi}\,\varphi_{0,-1}\varphi_{0,1}$ is the wavefunction overlap of the ground states of the harmonic oscillators,

$$q_{00} = \exp\left(-\frac{\hbar I_a^2}{4e^2E_L\omega_p}\right). \tag{4.8}$$

The current operator is however unaffected. Nevertheless, the average current in the junction is changed by the interaction with the LC-circuit. In equilibrium this average

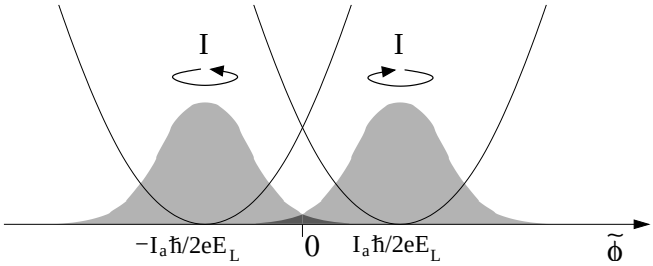

Figure 4.1: Schematic picture of the two harmonic oscillators, for the different current states of the point contact. The coupling is proportional to the overlap.

Josephson current is,

$$I_{eq} = \frac{e\Delta}{\hbar}\frac{D\sin\phi_e}{2E'_a(\phi_e)}, \tag{4.9}$$

where the renormalized spectrum of the Andreev states is given by,

$$E'_a(\phi) = \Delta\sqrt{\cos^2\frac{\phi}{2} - q_{00}^2 R\sin^2\frac{\phi}{2}}. \tag{4.10}$$

The change of the spectrum and the average current can be interpreted as the effect of the inert ring, which slows down the dynamics. Consider the situation $q_{00} \approx 1$, which corresponds to $\hbar\omega_p \gg (\frac{\Phi_0}{2\pi})^2 I_a^2/E_L \sim \Delta^2/E_L$. This case corresponds to a small capacitance C, *i.e.* a small particle mass in the mechanical analog of the circuit. Accordingly, it is easy for the qubit to switch the direction of the current and the dynamics of the qubit is almost unaffected by the LC-circuit. The situation is the opposite if the capacitance is large. The current states become non-fluctuating; the backscattering by the contact is suppressed.

If we combine the requirements we have used in the derivation, we can write the "working conditions" for the Andreev level qubit. These conditions are conveniently concluded as a chain of inequalities:

$$2\Delta\sqrt{R}q_{00} \ll \Delta\frac{\Delta}{E_L} < \hbar\omega_p \ll 4\Delta. \tag{4.11}$$

The average current carried by an arbitrary superposition of the Andreev states $|0\rangle$ and $|1\rangle$,

$$|\Psi\rangle = ae^{iE'_a t/\hbar}|0\rangle + be^{-iE'_a t/\hbar}|1\rangle, \tag{4.12}$$

is straightforward to calculate by taking the average of the current operator $\langle\Psi|\hat{I}|\Psi\rangle$, using the current operator in Eq. (4.5). The generally time dependent current is then,

$$I = I_{eq}(\phi_e)\left(|b|^2 - |a|^2 + 2\mathrm{Re}[ab^* e^{i2E'_a t/\hbar}]q_{00}\sqrt{R}\tan\frac{\phi_e}{2}\right). \tag{4.13}$$

Note that this result is different from the results presented in Paper IV where the interaction with the LC-circuit is not included.

The state of the Andreev level qubit can be read out either by measuring the induced flux or the current in the ring, using the technique based on macroscopic quantum tunneling developed by Cottet *et al.* [66], see below Sec. 5.1.

Single qubit operations

The Andreev level qubit has essentially two "knobs" for quantum manipulations, the external field and the transparency of the point contact. To set the qubit to zero (the ground state) is the easy part: we just switch the external field to zero $(\mathrm{mod}\ \Phi_0)$ and the Andreev states are forced out to the continuum. Hence, we can expect that quasiparticle excitation will relax the system immediately. Then we turn the external flux adiabatically to $\Phi_0/2$, with the qubit in the lower state.

The linear interaction with small variations in the external flux is given by

$$\hat{H}_i = I_a \delta\Phi_e(t)\sigma_z, \tag{4.14}$$

which is given by the expansion in Eq. (4.3), considering the qubit Hamiltonian in the current basis Eq. (4.7). Thus, the external field is a good method for inducing Rabi oscillations and to perform single qubit operations. If the frequency of the applied rf-signal is close to the resonant frequency $2E'_a/\hbar$, we get Rabi oscillations with the frequency,

$$\Omega = 2Aq_{00}\sqrt{R}D\frac{\Delta^2}{\hbar E'_a}\sin^2\frac{\phi}{2}, \tag{4.15}$$

where A is the amplitude of the applied rf-signal. Hence, the qubit can be set to any desired superposition by applying rf-pulses with appropriate length.

An alternative way to manipulate the qubit is to switch the external flux fast on the time scale of the qubit, $\hbar/2E'_a$. This method has both advantages and disadvantages. The advantages are that the method is simple and instant on the qubit time scale. The main disadvantage is that the switching not only induces transitions between the qubit states but generally also transitions to the continuum. The following calculation does not take into account the interaction with the loop and corresponds accordingly to $q_{00} = 1$.

The wave functions for the point contacts are straightforward to derive by solving Eq. (2.59). Consider, for example, electrons and holes, with energy within the gap, traveling to the right in the normal region, which corresponds to exponentially decaying electron-like and hole-like wave functions in the right superconductor, on the form Eq. (2.45) and with the wave vector in Eq. (2.49). The amplitudes for these states are,

$$a_\pm = \frac{1}{\sqrt{2}}\sqrt{1 \pm \mathrm{sign}\,(\sin\phi_e)\sqrt{1 - R\Delta^2/E_a^2}}, \tag{4.16}$$

where $(+)$ and $(-)$ denote electrons and holes, respectively, for $E > 0$. Note that, we only have to calculate the wave function in one of the electrodes since the junction is symmetric.

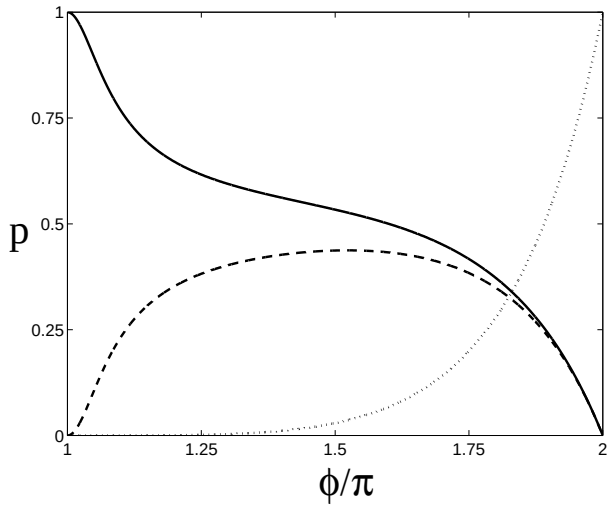

Figure 4.2: The probability to find the Andreev level qubit in the ground state (solid line) and the excited state (dashed line) after instant switching of the phase difference .The qubit was initially in the ground state at $\phi = \pi$ ($R = 0.01$). The leakage to the continuum, caused by the instant switching given by Eq. (4.20), is shown with the dotted line. [Fig. 2 in Paper IV]

The matrix elements for instant phase switching, $z_{\sigma_1,\sigma_2}(\phi_e^{(1)}, \phi_e^{(2)})$, are then the overlap of the wave functions before and after the phase is switched. If the qubit was initially in the ground state we have,

$$\begin{aligned} z_{-1,-1}(\phi_e^{(1)}, \phi_e^{(2)}) &= \chi(\phi_e^{(1)}, \phi_e^{(2)}) e^{-(\gamma_1-\gamma_2)/2} \\ &\quad \Big[a_+(\phi_e^{(1)}) a_+(\phi_e^{(2)}) \cos(i\frac{\gamma_1-\gamma_2}{2} + \frac{\phi_e^{(1)}-\phi_e^{(2)}}{4}) \\ &+ a_-(\phi_e^{(1)}) a_-(\phi_e^{(2)}) \cos(i\frac{\gamma_1-\gamma_2}{2} - \frac{\phi_e^{(1)}-\phi_e^{(2)}}{4}) \Big], \quad (4.17) \\ z_{-1,1}(\phi_e^{(1)}, \phi_e^{(2)}) &= \chi(\phi_e^{(1)}, \phi_e^{(2)}) e^{-(\gamma_1+\gamma_2)/2} \\ &\quad \Big[a_+(\phi_e^{(1)}) a_-(\phi_e^{(2)}) \sin(i\frac{\gamma_1+\gamma_2}{2} + \frac{\phi_e^{(1)}-\phi_e^{(2)}}{4}) \\ &- a_-(\phi_e^{(1)}) a_+(\phi_e^{(2)}) \sin(i\frac{\gamma_1+\gamma_2}{2} - \frac{\phi_e^{(1)}-\phi_e^{(2)}}{4}) \Big], \quad (4.18) \end{aligned}$$

where γ_i is given by Eq. (2.46), and

$$\chi(\phi_e^{(1)}, \phi_e^{(2)}) = \frac{2\sqrt{\xi(\phi_e^{(1)})\xi(\phi_e^{(2)})}}{\xi(\phi_e^{(1)}) + \xi(\phi_e^{(2)})}. \quad (4.19)$$

The probability to end up in the continuum is determined by $p_{-1,\mathrm{cont}} = 1 - |z_{-1,-1}|^2 - |z_{-1,1}|^2$. In contrast to the matrix elements for transitions between the Andreev levels, this expression is rather simple and independent of R,

$$p_{-1,\mathrm{cont}}(\phi_e^{(1)}, \phi_e^{(2)}) = 1 - |\chi(\phi_e^{(1)}, \phi_e^{(2)})|^2. \quad (4.20)$$

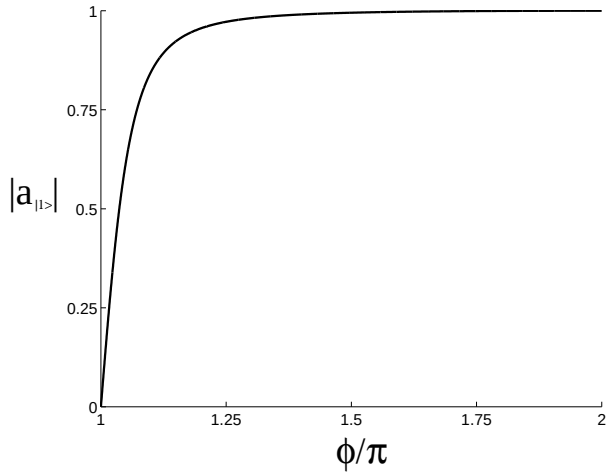

Figure 4.3: The amplitude of the excited state after an instant switching of the phase difference from ϕ to $2\pi - \phi$. The qubit was initially in the ground state ($R = 0.01$). There is no leakage to the continuum.

For switching from the working point, $\phi_e = \pi$, to some other phase the leakage to the continuum is rather large, see Fig. 4.2. Hence, this way of manipulating the qubit is not appropriate for coherent operations.

A more appealing situation appears if the qubit is switched symmetrically around π, $\phi_e \to 2\pi - \phi_e$. Then the leakage to the continuum states is zero, and the switching probability is given by the simple formula, which is straightforward to derive from Eq. (4.18),

$$p_{-1,1} = 1 - \frac{R}{E_a^2(\phi_e)} \sin^2 \frac{\phi_e}{2}, \tag{4.21}$$

where $p_{-1,1} = |z_{-1,1}|^2 = 1 - |z_{-1,-1}|^2$. Using this method, it is possible to obtain any superposition of the qubit states by a single switch of the phase. The modulus of the amplitude for the excited state after a switch from ϕ_e to $2\pi - \phi_e$ is shown in Fig. 4.3. When the desired superposition is obtained the qubit can be switched adiabatically back to the working point at $\phi_e = \pi$.

The second way of manipulating the qubit, by controlling the transparency, is a straightforward way to control the σ_x-term in the Hamiltonian and hence the fluctuations between the current states (if the transparency is switched adiabatically). It is also possible to induce transitions by non-adiabatic variation of the transparency. The corresponding interaction Hamiltonian is non-diagonal, $H_I \sim \delta R \sigma_x$ (in the current basis).

Coupling of qubits

Coupling of qubits is important, both for the applications in future quantum electronics and since coupled qubits open the way to experiments with entangled qubits, for example test of Bell-like inequalities [95].

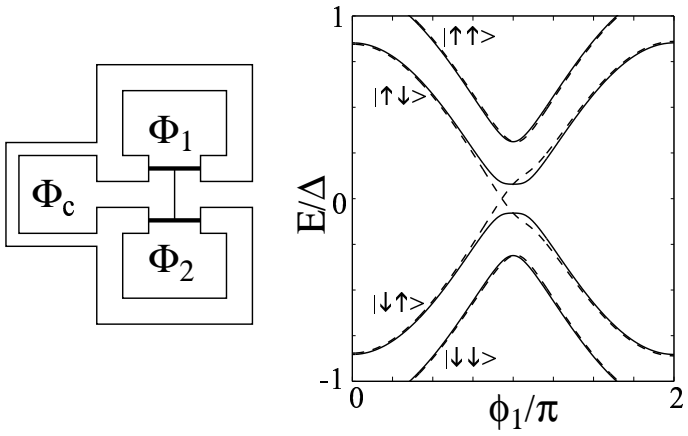

Figure 4.4: The double qubit device, with direct coupling of the normal regions and the corresponding two-particle spectrum. The flux through the control loop can be used to control the coupling. The parameters are $D_1 = D_2 = 0.97$, $T = 0.01$ and $\phi_2 = 0.93\pi$. The solid line corresponds to coupled qubits ($\phi_c = \pi/2$) and the dashed line corresponds to uncoupled qubits ($\phi_3 = 0$). [Fig. 3 in Paper IV]

Perhaps, the most natural way to couple the qubits is by mutual inductance. This yields a weak σ_z-coupling of the qubits. The slow dynamics of the qubits can be calculated using a similar approach as for the single Andreev level qubit [96].

In Paper IV another type of coupling is suggested: direct coupling of two point contacts in a four-terminal junction. The setup is appealing since the flux through the control loop (see Fig. 4.4), which determines the relative phase difference between the two qubit rings, offers an extra knob, which can be used to control the coupling.

The derivation of the Andreev spectrum of the four-terminal junction is rather straightforward. We employ a simple scattering matrix for the four-terminal contact,

$$S = \begin{pmatrix} r_1 & d_1 & \sqrt{T} & \sqrt{T} \\ d_1 & r_1 & \sqrt{T} & \sqrt{T} \\ \sqrt{T} & \sqrt{T} & r_2 & d_2 \\ \sqrt{T} & \sqrt{T} & d_2 & r_2 \end{pmatrix}. \tag{4.22}$$

Then we proceed in the same manner as in the case of the SNS interferometer and define new scattering amplitudes at both sides, by employing the unitary transformation which was used to reduce the SNS interferometer to an effective 2-terminal junction, see Sec. 3.2. This yields an effective two-terminal SNS junction with transfer matrices similar to Eq. (3.3) describing the scattering at both the effective SN interfaces, and an effective impurity with transparency $2T$ in between. Then we can follow the approach of Sec. 2.2 to calculate the spectrum. However, this new system is more complicated due to the normal scattering at the effective SN interfaces, which yields a 4 by 4 linear equation system for the scattering amplitudes. To find the spectrum we have to

calculate the determinant of this 4 by 4 matrix. The resulting spectrum is,

$$E^2 = \Delta^2 - \frac{\tilde{D}}{D_1 D_2 (1+\tilde{T})}\Big[\xi_+^2 \ \pm \ \sqrt{\xi_-^4 - \tilde{T}\xi_2^2\xi_1^2}\Big], \tag{4.23}$$

where $\xi_i^2 = \Delta^2 - E_a^2(\phi_{e,i})$, $\phi_{e,i}$ is the dimensionless external flux in ring $i = 1, 2$, and

$$\begin{aligned}
\xi_\pm^2 &= \frac{\xi_1^2 \pm \xi_2^2}{2} + T(1 - \cos\phi_c \cos\frac{\phi_{e,1}}{2}\cos\frac{\phi_{e,2}}{2}), \\
\tilde{D} &= (D_1 + T)(D_2 + T) - T\cos^2\theta_+, \\
\tilde{T} &= \frac{T}{D_1 D_2}(T + 2\tilde{D} \\
&+ \sqrt{[(R_1 + T)(D_2 + T) - T\sin^2\theta_+][(R_2 + T)(D_1 + T) - T\sin^2\theta_+]}),
\end{aligned}$$

where $\theta_+ = (\theta_1 + \theta_2)/2$ and $\theta_i = \mathrm{Arg}[r_i - d_i]$. Although this spectrum looks rather complicated, it is straightforward to see that Eq. (4.23) yields the ordinary spectrum of two uncoupled qubits, $E^2 = \Delta^2 - \xi_i^2$, when $T \to 0$. The spectrum of the double qubit is shown in Fig. 4.4, which also shows the possibility to switch off the hybridization of the levels using the control flux Φ_c, provided that the two qubits have the same transparency, $D_1 = D_2$. Moreover, if the two qubits are weakly coupled we can expand Eq. (4.23) in T, which yields the simplified spectrum,

$$E^2 = E_+^2 \pm \sqrt{E_-^4 + TD\Delta^4[(\tilde{\phi}_1 - \tilde{\phi}_2)^2 + 2\tilde{\phi}_1\tilde{\phi}_2\sin^2(\phi_c/2)]}, \tag{4.24}$$

where $E_\pm^2 = [E_a^2(\phi_{e,1}) \pm E_a^2(\phi_{e,2})]/2$ and $D_1 = D_2$. The deviation from the degeneracy point is given by $\tilde{\phi}_i = \phi_{e,i} - \pi$, and assumed to be small $\tilde{\phi}_i \ll 1$. The role of the control flux is clear from Eq. (4.24); the hybridization vanishes at $\phi_c = 0$.

The theory presented above does not include any interaction with fluctuating fluxes in the rings. This interaction, which will be the subject of a future work, will remove the symmetry of the spectrum given by Eq. (4.23), which will make control-NOT operations possible to perform.

CHAPTER 5

READOUT OF PERSISTENT CURRENT QUBITS

In this chapter I discuss recent results on readout of macroscopic qubits where the two-level system couples to the current in a superconducting ring, such as the Andreev level qubit. The work is done in collaboration with V. Shumeiko, A. Zazunov, G. Johansson and G. Wendin.

5.1 READOUT USING MACROSCOPIC QUANTUM TUNNELING

We consider a *persistent current qubit*, *i.e.* a phase qubit or a charge qubit where the states of the two-level system couples to the current in a superconducting ring. The model we use is relevant for flux qubits, like Leggett's rf-SQUID [58, 60], the flux qubit by Mooij *et al.* [67], and the Andreev level qubit, but also for the more recent charge-phase qubit by Cottet *et al.* [66].

We consider a readout device consisting of a large Josephson junction, which is inserted in the superconducting ring of the qubit. This readout technique was suggested by Cottet *et al.* [66] and has recently been experimentally tested by Vion *et al.* [69]. The Meter (the large Josephson junction) is also connected to a stable current generator and an accurate voltmeter, see Fig. 5.1. We require that the critical current in the Meter is large compared to the circulating current in the ring, in order to minimize the back action, $E_{Jm} \gg E_J$, where E_{Jm} is the Josephson energy of the Meter and E_J the effective Josephson energy of the qubit.

The readout scheme is the following: the measurement is performed by increasing the bias current I_b adiabatically to a peak value near the critical current I_{cm} of the Meter for a finite time τ, which yields a significant probability for Macroscopic quantum tunneling (MQT). Since the MQT-rate depends on the total current through the Meter, $I_b + I$, it will also depend on the sign and the amplitude of the current in the ring, I. For the ideal meter the MQT-rates, corresponding to the two qubit states, are very different. We may then chose the time τ such that one state is stable with certainty, while the other state decays with high probability during the time τ. A signal on the voltmeter, due to an MQT-event, tells us that the qubit was in the unstable state. If no signal appeared on the voltmeter, during the time current bias was turned on, the qubit was in the stable state. In both cases, coherence is lost and we know the state of the

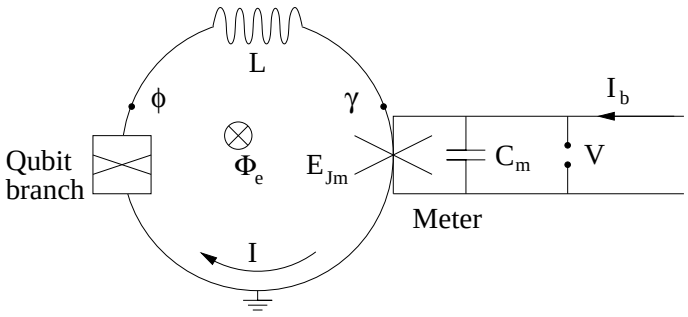

Figure 5.1: Schematic picture of the qubit, here an rf-SQUID, and the Meter. The current supply to the Meter are constructed to avoid induced flux in the SQUID-ring by the bias current.

qubit.

We consider a generalized model for the persistent current qubit and the Meter, schematically shown in Fig. 5.1. The device consist of a *qubit branch* and a *Meter branch* connected via the inductance L. The qubit branch consists of the Josephson junction(s) or the point contact of the qubit. The phase drop over the Meter is γ and the phase drop over the qubit branch is ϕ. The flux dependence of the qubit phase ϕ is given by the equation $(\phi - \gamma) = (2\pi/\Phi_0)(\Phi_e + LI) \pmod{2\pi}$, where Φ_e is the external flux.

To describe the circuit we employ the technique of branch fluxes, see *e.g.* [97]. We can write the Lagrangian of the device as

$$L = L_\phi(\phi) - \frac{E_L}{2}(\phi - \gamma - \phi_e)^2 + \left(\frac{\Phi_0}{2\pi}\right)^2 \frac{C_m}{2}\dot{\gamma}^2 + E_{Jm}\left[\cos\gamma + \frac{I_b}{I_{cm}}\gamma\right], \quad (5.1)$$

where $L_\phi(\phi)$ is the Lagrangian of the junctions in the qubit branch, C_m is the capacitance of the Meter and $E_L = (\Phi_0/2\pi)^2/L$. It is straightforward to proceed with the Legendre transformation to achieve the full Hamiltonian, which is quantized in the usual way, using the dynamical variables,

$$\begin{aligned} \tilde{\gamma}(t) &= \gamma(t) - \gamma_0 \\ \tilde{\phi}(t) &= \phi - \phi_{e1}, \end{aligned}$$

where $I_b = I_{cm}\sin\gamma_0$ defines the local minimum in the "tilted washboard potential" of the Meter, and $\phi_{e1} = \phi_e + \gamma_0$ determines the effective external flux seen by the qubit branch.

If we separate the terms depending on $\tilde{\phi}$, which yields the qubit Hamiltonian $\hat{H}_q$, from the $\tilde{\gamma}$-dependent terms of the Meter we get,

$$\hat{H} = \hat{H}_q(\tilde{\phi}) + \hat{H}_i + \hat{H}_m(\tilde{\gamma}), \quad (5.2)$$

where

$$\hat{H}_m = \frac{q_{\tilde{\gamma}}^2}{2C_m} + \frac{\epsilon_m}{2}\tilde{\gamma}^2\left(1 - \frac{2\tilde{\gamma}}{3\gamma_b}\right) + \frac{E_L}{2}\tilde{\gamma}^2 \quad (5.3)$$

$$\hat{H}_i = -E_L\tilde{\phi}\tilde{\gamma} = -\frac{\Phi_0}{2\pi}\hat{I}_l\tilde{\gamma}, \quad (5.4)$$

where $\epsilon_m = E_{Jm}\sqrt{1 - I_b^2/I_{cm}^2}$, $\gamma_b = 2\sqrt{I_{cm}^2/I_b^2 - 1}$, $q_{\tilde{\gamma}} = -i2e\partial_{\tilde{\gamma}}$ and $q_\phi = -i2e\partial_{\tilde{\phi}}$. The operator for the current in the ring is $\hat{I}_l = (\Phi_0/2\pi)\tilde{\phi}/L$. In Eq. (5.3) we have expanded the Hamiltonian of the Meter around $\tilde{\gamma} = 0$, in the usual way for calculation of MQT-rates [98]. The expansion in the parameter $\tilde{\gamma}$ is valid if the Josephson energy of the Meter is large $E_{Jm} \gg \hbar\omega_m$, where $\hbar\omega_m = \sqrt{2\epsilon_m E_{Cm}}$, and if $E_L \gg \hbar\omega_m$, which ensure the ground state is localized although $I_b = 0$. Provided that $E_{Jm} \gg E_J$ we can treat the fluctuations of the Meter as a small perturbation to the qubit.

In Appendix B the reduced two-level Hamiltonian for the rf-SQUID is derived, Eq. (B.7), and the reduced current operator, Eq. (B.8). The derivation of the two-level Hamiltonian, Eq. (C.6), as well as the current operator, Eq. (C.7), for the charge-phase qubit developed by Cottet *et al.* [66] is found in Appendix C. Finally, the current operator, Eq. (4.5), and the Hamiltonian, Eq. (4.7), for the Andreev level qubit are presented in Chapter 4. The Andreev qubit Hamiltonian including the Meter branch is obtained by replacing the external flux ϕ_e with the effective external flux $\phi_{e1} = \phi_e + \gamma_0$, in Eq. (4.7). Note that, for the two-level system the reduced current operators $\hat{I}_l$ and $\hat{I}$, Eq. (4.5), are identical. Generally, we use the conventional spin representation for the qubit Hamiltonian,

$$\hat{H}_q = h_x\sigma_x + h_z\sigma_z, \tag{5.5}$$

which is written in the eigenbasis of the reduced current operator, $\hat{I} = I_q\sigma_z$.

Slow dynamics of the qubit and the Meter

If we consider the regime, $I_b \ll I_{cm}$, where the rate of MQT is negligible, the Hamiltonian for the system of the qubit and the Meter can be reduced to a simple two-level form.

In the case $I_b = 0$, the two states of the qubit Hamiltonian correspond to two displaced identical harmonic oscillators, where the displacement is given by

$$\langle\gamma\rangle_0 = \gamma_0 \pm \tilde{\phi}_0, \quad \tilde{\phi}_0 = \frac{I_q E_J}{I_c E_{Jm}}(1 - I_b^2/I_c^2)^{-1/2}, \tag{5.6}$$

where $<>_0$ denotes the average over zero point fluctuations and $\pm$ denotes the state of the qubit. This displacement is the Pointer in the Meter.

If the plasma frequency of the Meter is large, $\hbar\omega_m \gg E_q = \sqrt{h_x^2 + h_z^2}$, the wave functions of the harmonic oscillators can be approximated with the ground state wave functions, and we can integrate out the $\tilde{\gamma}$-degree of freedom using the same method as in Sec. 4.1 [77]. We arrive at the effective two-level Hamiltonian,

$$\hat{H} = h_z\sigma_z + h_x g_{00}\sigma_x, \tag{5.7}$$

where g_{00} is the overlap of the two ground states,

$$q_{00} = \exp\left(-\frac{I_q^2}{I_c^2}\frac{E_J^2}{\hbar\omega_m\epsilon_m}\right). \tag{5.8}$$

This renormalization of the qubit dynamics depends on which qubit we consider. The rf-SQUID characteristics obey the condistins (see Appendix B), $E_{Jm} \gg E_L \gg \hbar\omega_p$, and $E_J \sim E_L$. Hence, q_{00} is not necessarily close to unity. The Andreev level qubit is in a similar situation, since $E_J \sim \Delta \gg \hbar\omega_m$. The situation is different for the charge-phase qubit [66] (see Appendix C): for this qubit we have both $E_{Jm} \gg E_J$ and $\hbar\omega_m \gg E_J$, which ensures that q_{00} is always close to unity, and the renormalization is not important.

The measurement

Our aim is to read out the information about the state of the qubit as fast and as accurate as possible. This process includes necessarily two steps, associated with the time τ_r for the ramping of the bias current and the time τ when the bias current is kept constant at the peak value. Preferably, the ramping time τ_r should be short compared to the inverse MQT-rate of the unstable state. The lower limit is set by the adiabatic approximation regarding the Meter, which requires $\tau_r \gg 1/\omega_m$. The switching-on of the Meter shifts the effective external flux away from the working point to a point at $\phi_{e1} = \phi_e + \gamma_0(I_b)$. This readout point can be adjusted by changing the external flux at the same time as the current bias.

Consider the system when $I_b > 0$. Up to an unimportant constant energy term Eq. (5.2) can be rewritten as

$$\begin{aligned} \hat{H} &= \begin{pmatrix} h_z + H_+ & h_x \\ h_x & -h_z + H_- \end{pmatrix}, \\ H_\sigma &= \frac{q_{\tilde{\gamma}}^2}{2C_m} + \frac{\epsilon_\sigma}{2}\gamma^2(1 - \frac{2\gamma}{3\gamma_{b\sigma}}), \end{aligned} \tag{5.9}$$

where $\sigma = \pm 1$, $\gamma_{b\sigma} = \sqrt{\gamma_b^2 - 4\sigma\tilde{\phi}_0\gamma_b}$, $\epsilon_\sigma = \epsilon_m\gamma_{b\sigma}/\gamma_b$, and the displacement, $\tilde{\phi}_0 \ll 1$, is given by Eq. (5.6). Although the potential of the Meter is no longer harmonic we assume that the harmonic approximation is still valid for the lowest energy levels. There is however a finite rate for MQT even for the lowest levels, which is different for the two qubit states due to the displacement.

Assuming zero temperature the MQT rates for the qubit states are given by the standard expression [98],

$$\Gamma_\sigma = \omega_\sigma\sqrt{60}\sqrt{\frac{S_\sigma}{2\pi\hbar}}e^{-S_\sigma/\hbar}, \tag{5.10}$$

where

$$\begin{aligned} S_\sigma &= (6/5)\frac{\epsilon_\sigma}{\omega_\sigma}\gamma_{b\sigma}^2 \\ &\approx 12\frac{E_{Jm}}{\omega_m}\Big[\frac{2}{5}(I_{cm}^2/I_b^2 - 1) - \sigma I_q/I_b\Big]. \end{aligned} \tag{5.11}$$

To achieve a good signal-to-noise ratio of the readout we require that

$$\Gamma_+ \gg \Gamma_-, \Gamma_r, \tag{5.12}$$

where Γ_r is the relaxation rate of the qubit due to interaction with the environment. Hence, the bias current should be ramped to a peak value where the MQT-rate for the "unstable" state is much larger than the relaxation rate, but not so high that the probability for the "stable" state to tunnel gets significant during the time τ. Since the dependence of the action S_σ in Eq. (5.11) is dominated by the exponential factor, we can estimate the ratio between the MQT rates,

$$\frac{\Gamma_+}{\Gamma_-} \sim \exp\left(24\frac{E_{Jm}}{\hbar\omega_m}\frac{I_q}{I_b}\right). \tag{5.13}$$

00.00, Swedish time, south of el Calafate in Argentina, Jan 1 2000. We have had our third flat tire on our little Hunday-bus, and the jack is still too small. The road is straight, of doubtable quality and continues to the horizon where the Patagonian sky meets the desert-like southern pampas.

00.30, local time, in el Calafate. The new millennium was celebrated with champagne from Chile and fireworks; PJ re-ignited the grill using a bottle of camping fuel. He survived. Now, we are strolling around in el Calafate. El Calafate is a small yet rather strange city, located on the flatland east of the Andes on the shore of lake Argento. There are more flamingos than people in this part of the world. Nevertheless, an increasing number of tourists spend one or two nights on some of the towns dry campings, waiting for the bus to the famous national park *los Glaciares* in the Andes some 80 km to the west. Other people, like us, are repairing their flat tires. Everything is expensive, and there is no real bank.

The first hour of the new millennium is rather quiet. Suddenly a line of honking cars appears. This is apparently Calafates official millennium party. The first car is a pick-up where the basket of a hot air balloon has been mounted on the board. A drunk and happy pilot is standing in the basket, firing yellow bursts from the four burners. Like a carnival without dancers the line of dirty cars drives slowly back and forth on the main street.

ACKNOWLEDGMENTS

Nu är det dags att för mig tacka alla er som har hjälpt mig att göra denna avhandling möjlig.
Först vill jag tacka min handledare *Vitaly Shumeiko* för allt stöd och all hjälp under mina år som doktorand, och för alla intressanta diskussioner.
Alex Zazunov and *Katya Bratus'*, I thank especially for being great inspiring cooperators during two of the projects. There are many aspects of the *Ukrainian style of physics*. Its only rock'n roll, but I like it!
Vidare går min tacksamhet till *Göran Wendin*, professor i vår grupp, för hjälp och support.
Stort tack också till mina doktorandkollegor, för ert trevliga sällskap, alla intressanta fysikdiskussioner, alla intressanta diskussioner om annat här i världen, och all kaka: *Åke Ingerman*, *Göran Johansson*, *Peter Samuelsson*, *Thomas Löfvander*, *Andreas Käck*, *Ingela Malmberg*, *Anton Grigoriev* and *Jonas Sköldberd*. Förlåt, Göran, Peter och Thomas, ni är ju inte doktorander längre, utan doktorer, fast ni hamnar ändå i samma lista. På det hela taget har mina fem år som doktorand varit en intressant och trevlig erfarenhet. Jag har vuxit som fysiker, människa och alpinist.
Höll nästan på att glömma bort att tacka dig *Veronika*. Jag lovar att fixa ringproblemet nu när jag har mer tid!

Göteborg, March 2002, *Jonn Lantz*

APPENDIX A

THE HUBBARD-STRATONOVICH PROCEDURE

The Hubbard-Stratonovich procedure is an analytical method of rewriting the effective action of a physical system, using functional integrals [73, 76]. A good introduction to functional integration can be found in [99], which also includes an introduction to Grassman fields and the integration rules for Grassman fields. In fact, the anti-commutating rules for Grassman fields makes functional integration very easy.

One of the most important properties of functional integrals is the invariance with respect to shifts of the integration variable,

$$\int D\eta^\dagger D\eta\, e^{-\int dx_1 dx_2\, \eta^\dagger(x_1) A \eta(x_2)} = \int D\eta^\dagger D\eta\, e^{-\int dx_1 dx_2\, (\eta^\dagger(x_1)+\theta_1^\dagger(x_1)) A (\eta(x_2)+\theta_2(x_2))}. \tag{A.1}$$

Since $\eta^2 = 0$ for any Grassman variable, functions of Grassman numbers can be Taylor-expanded to first order, without any approximation made. Hence, all integrations will be simple. The ordinary integral over a Grassman number is defined as

$$\int d\eta\, f(\eta) = \int d\eta\, (a + b\eta) = b, \tag{A.2}$$

where a and b are the first Taylor coefficients of the function $f(\eta)$. It is easy to show that this definition yields the desired invariance to shifts of the integration variable. Moreover, to handle products of integrals a sign convention is nessecary, $\int d\eta_2 d\eta_1\ \eta_1\eta_2 = +1$, performing the innermost integral first.

The functional integral over an action which depends on a Grassman field is evaluated by replacing the x-integral with a finite sum over a large number of intervals, δx, after which each term in the sum can be evaluated separately.

$$\int D\eta^\dagger D\eta\, e^{-\int dx_1 dx_2\, \eta^\dagger(x_1) A \eta(x_2)} = \left(\prod_i \int d\eta_i^\dagger d\eta_i\right) e^{-\sum_{ij} \delta x^2 \eta_i^\dagger A_{ij} \eta_j} = \prod_i a_i = \mathrm{Det}\ A, \tag{A.3}$$

where A is an operator with the eigenvalues a_i. The diagonalization of the operator A can be made since the functional integral is invariant to unitary transformations of the fields. The normalization constant, containing the product of the x-intervals, is unimportant and omitted.

The validity of the Hubbard Stratonovich procedure is a direct consequence of the invariance Eq. (A.1). The field transformation allows us to introduce new fields and decouple others, which is very useful. The procedure to decouple two Grassman fields η and μ is

$$
\begin{aligned}
& e^{\int dx_1 dx_2\, \eta^\dagger(x_1) A \mu(x_2)} = \\
& \mathrm{Det}\, A \int D\theta_1^\dagger D\theta_2\, e^{\int dx_1 dx_2\, [\eta^\dagger(x_1) A \mu(x_2) - (\theta_1^\dagger(x_1) - \eta^\dagger(x_1) A) A^{-1} (\theta_2(x_2) - A\mu(x_2))]} \\
& = \mathrm{Det}\, A \int D\theta_1^\dagger D\theta_2\, e^{-\int dx_1 dx_2\, [\theta_1^\dagger(x_1) A^{-1} \theta_2(x_2) + \theta_1^\dagger(x_1) \mu(x_2) + \eta^\dagger(x_1) \theta_2(x_2)]}. \qquad \text{(A.4)}
\end{aligned}
$$

APPENDIX B

TWO-LEVEL HAMILTONIAN OF THE HYSTERETIC RF-SQUID

In this appendix I present a derivation of the reduced two-level Hamiltonian of the rf-SQUID, near the degeneracy point $\phi_e = \pi$. The parameters are defined in line with the analysis in Sec. 5.1 and Fig. 5.1, with a single Josephson junction associated with the qubit branch. With appropriate parameters; $E_J \sim E_L$ and $\Phi_e \approx \Phi_0/2$, the effective potential takes the form of a double well, as shown in Fig. B.1.1. The Hamiltonian of the rf-SQUID is obtained

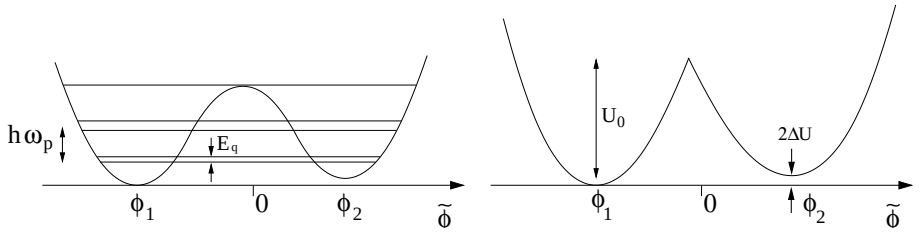

Figure B.1: Schematic pictures of the potential of the rf-SQUID for $E_J/E_L \approx 2$ and with $\phi_e \approx 1.01\pi$ (left) and the model potential (right). The plasma frequency is assumed large compared to the level splitting $2\Delta U$ of the two-level system.

form Eq. (5.1), by replacing the qubit branch with one Josephson junction and its effective capacitance C,

$$\hat{H}_q = \frac{q_{\tilde{\phi}}^2}{2C} - E_J \cos(\tilde{\phi}(t) + \phi_{e1}) + \frac{E_L}{2}\tilde{\phi}(t)^2, \tag{B.1}$$

where $q_{\tilde{\phi}} = -i2e\partial_{\tilde{\phi}}$. The minima of the double well potential are given by

$$E_L\tilde{\phi} + E_J \sin(\tilde{\phi} + \phi_{e1}) = 0. \tag{B.2}$$

Accordingly, we define $\tilde{\phi} = \phi_1 < 0$ at the left minimum and $\tilde{\phi} = \phi_2 > 0$ at the right minimum. In order to make the potential in Eq. (B.1) easier to handle we replace it with a model potential defined by

$$\begin{aligned} U(\tilde{\phi}) &= U_1 + U_2 \\ U_1 &= \frac{\epsilon_u}{2}\tilde{\phi}(\tilde{\phi} - 2\phi_1)\theta(-\tilde{\phi}) \\ U_2 &= \frac{\epsilon_u}{2}\tilde{\phi}(\tilde{\phi} - 2\phi_2)\theta(\tilde{\phi}), \end{aligned}$$

where $\epsilon_u = E_L + E_J \cos(\phi_{e1} + \phi_2)$, required that $\phi_e - \pi \ll 1$. The energy difference between the bottoms of the two wells is given by

$$\Delta U = \frac{\epsilon_u}{4}(\phi_2^2 - \phi_1^2) \tag{B.3}$$

and the mean depth, compared to $U(0)$, is

$$U_0 = \frac{\epsilon_u}{4}(\phi_1^2 + \phi_2^2). \tag{B.4}$$

Note that $U_0 \sim E_L \sim E_J$. We consider the case $U_0 \gg \hbar\omega_p$, where $\hbar\omega_p = \sqrt{2E_C\epsilon_u}$, when the harmonic approximation is valid for the lowest energy levels in each well.

A well defined two-level system is obtained near the degeneracy point, $\phi_e = \pi$, required that $\hbar\omega_p/2 \gg E_q$, where $2E_q$ is the minigap of the two-level system. If we restrict to zero temperature and the ground state in each harmonic oscillator, we can write the state of the system as a superposition,

$$|\Psi\rangle = a|1\rangle + b|2\rangle, \tag{B.5}$$

where $|i\rangle$ are the ground states of the harmonic oscilators, $i = 1, 2$. Then we project the Heisenberg equation with the Hamiltonian $H = q_{\tilde{\phi}}^2/2C + U(\tilde{\phi})$ onto these states,

$$\begin{aligned} i\hbar\dot{b} + i\hbar\dot{a}\langle 2|1\rangle &= b\langle 2|U_1|2\rangle + a\langle 2|U_2|1\rangle \\ i\hbar\dot{a} + i\hbar\dot{b}\langle 1|2\rangle &= b\langle 1|U_1|2\rangle + a\langle 1|U_2|1\rangle \end{aligned}$$

The overlap, neglecting terms of the order ΔU, is

$$\langle 1|2\rangle = \int d\phi\, \langle 1|\phi\rangle\langle\phi|2\rangle = e^{-\frac{2U_0}{\hbar\omega_p}} \tag{B.6}$$

We can then write the equation for the two-level system on the more convenient form, to leading order in $\langle 1|2\rangle$ and ΔU,

$$\begin{aligned} i\hbar\dot{b} &= b\Delta U + ah_x \\ i\hbar\dot{a} &= bh_x - a\Delta U. \end{aligned} \tag{B.7}$$

This equation can be mapped on Eq. (5.5), where $h_z = \Delta U$ and $h_x \approx \langle 1|2\rangle U_0/2$

The current operator, defined by $\hat{I}_l = (\Phi_0/2\pi)\tilde{\phi}/L$, is reduced in a similar way, keeping terms to leading order in $\langle 1|2\rangle$,

$$\begin{aligned} \langle 2|\hat{I}_l|\Psi\rangle &\approx b\frac{\Phi_0}{2\pi L}\langle 2|\tilde{\phi}|2\rangle = b\frac{\Phi_0}{2\pi}I_q \\ \langle 1|\hat{I}_l|\Psi\rangle &\approx a\frac{\Phi_0}{2\pi L}\langle 1|\tilde{\phi}|1\rangle = -a\frac{\Phi_0}{2\pi}I_q \end{aligned}$$

where $I_q = (\Phi_0/2\pi L)\phi_2$. Hence, we can write the two-level current operator as

$$\hat{I}_l = I_q(\phi_{e1})\sigma_z. \tag{B.8}$$

We can summarize the necessary inequalities as:

$$\begin{aligned} &E_J \sim E_L \gg \hbar\omega_p, \hbar\omega_m \gg E_q, \\ &\Delta \gg \hbar\omega_m, \hbar\omega_p, \end{aligned}$$

where $\hbar\omega_m$ is the plasma frequency of the Meter, see Sec. 5.1. Note that the first inequality implies $\phi_e - \pi \ll 1$.

APPENDIX C

THE CHARGE-PHASE QUBIT

In this appendix I present a derivation of the reduced Hamiltonian for the qubit used by Vion *et al.* [66, 69], formally referred to as the charge-phase qubit. The design is similar to the rf-SQUID but the device is operated in the regime $E_L \gg E_J$. The qubit is modeled by replacing

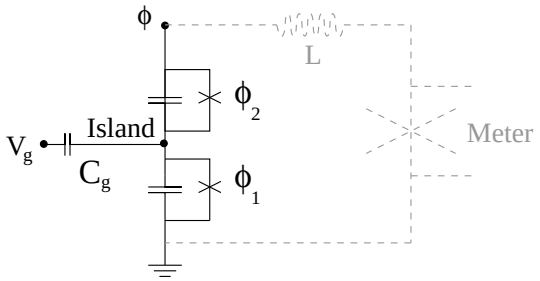

Figure C.1: Schematic picture of the achieve elements in the charge-phase qubit. The $(-)$-pole of the battery, V_g, is assumed to be contacted to the point $\phi/2$.

the qubit branch in Fig. 5.1 with two Josephson junctions, with (the same) Josephson energy E_J and capacitance C. Hence, $\phi = \phi_1 + \phi_2$. Moreover, the small island which is created between the junctions is coupled to a voltage source, via a weak capacitance $C_g \ll C$. We assume that the $(-)$-pole of the voltage bias V_g is attached to the superconducting ring in such a way that the charge on the gate capacitor is $Q_g = C_g(V_g + (\hbar/2\pi)\dot{\phi}/2)$, compared to ground. The current in the gate, $I_g = \dot{Q}_g$, is neglected.

The Lagrangian for the qubit branch is

$$L_\phi = \left(\frac{\Phi_0}{2\pi}\right)^2 \left[\frac{C_g}{2}(\dot{\phi}_v + \dot{\phi}/2 - \dot{\phi}_1)^2 + \frac{C}{2}(\dot{\phi}_1^2 + \dot{\phi}_2^2)\right] + E_J[\cos(\phi_1 + \phi_{e1}) + \cos(\phi_2 + \phi_{e1})]$$
$$= \left(\frac{\Phi_0}{2\pi}\right)^2 \left(\frac{C_g}{2}(\dot{\phi}_v - \dot{\phi}_-)^2 + \frac{2C}{2}\dot{\phi}_-^2 + \frac{C'}{2}\dot{\phi}^2\right) + 2E_J \cos(\frac{\phi_{e1} + \tilde{\phi}}{2}) \cos\phi_-, \qquad \text{(C.1)}$$

where $\dot{\phi}_v = (2e/\hbar)V_g$, $\phi_- = (\phi_1 - \phi_2)/2$ and $C' = C/2$. If we insert this Lagrangian in Eq. (5.1) we get the qubit Hamiltonian,

$$H_q = \frac{(Q_- - q)^2}{2C_t} + \frac{Q^2}{2C'} - 2E_J \cos(\frac{\phi_{e1} + \tilde{\phi}}{2}) \cos\phi_- + \frac{E_L}{2}\tilde{\phi}^2. \qquad \text{(C.2)}$$

where $C_t = 2C + C_g$, Q_- and Q are the conjugate quasi charges to ϕ_- and ϕ, respectively, and $q = -C_g V_g$ is the (static) charge induced by the gate capacitor. We quantize the Hamiltonian by imposing the commutation relations $[n, \phi_-] = i$, where $Q_- = 2ne$, and $[Q, \tilde{\phi}] = 2ie$ and use the operators $n = -i\partial_{\phi_-}$ and $Q = -2ie\partial_{\tilde{\phi}}$.

If $E_L \gg E_C$, where $E_C = (2e)^2/2C_t$, the fluctuations in $\tilde{\phi}$ are small and it is relevant to expand the Hamiltonian in $\tilde{\phi}$. Moreover, we let $\cos\phi_- \rightarrow \frac{1}{2}\sum_n (|n\rangle\langle n+1| + |n+1\rangle\langle n|)$ which follows from the commutation relation $[n, \phi_-] = i$. Using the n-basis we arrive at the qubit Hamiltonian

$$\begin{aligned}\hat{H}_q &= \sum_n \Big[(\frac{Q^2}{2C'} + \frac{E_L}{2}\tilde{\phi}^2)|n\rangle\langle n| + \frac{(2ne-q)^2}{2C_t}|n\rangle\langle n| \\ &- [2E_J\cos\frac{\phi_{e1}}{2} - \tilde{\phi}E_J\sin\frac{\phi_{e1}}{2}](|n\rangle\langle n+1| + |n+1\rangle\langle n|)\Big]. \end{aligned} \tag{C.3}$$

The full Hamiltonian is intractable, but we note that the limit, $E_L \gg E_C$, yields a weak coupling of the loop and the island. We can then estimate the level splitting by calculating the spectrum for the free island,

$$\hat{H}_{is} = \sum_n \Big[\frac{(2ne-q)^2}{2C_t}|n\rangle\langle n| - 2E_J\cos(\phi_{e1}/2)(|n\rangle\langle n+1| + |n+1\rangle\langle n|)\Big]. \tag{C.4}$$

The minimum level splitting for the two lowest levels is found at the degeneracy point, $q \approx e$, where the gap is of the order $2E_q \sim 4E_J\cos(\phi_{e1}/2)$. The distance to the third level is of the order of E_C. Thus, we require $E_C \gg E_J\cos(\phi_{e1}/2)$ for qubit operations. Under these assumptions we can restrict the analysis to the 2 lowest levels. Using the basis $|\sigma\rangle = (|0\rangle - \sigma|1\rangle)/\sqrt{2}$, where $\sigma = \pm 1$, we get the Hamiltonian [100],

$$\hat{H} = \frac{Q^2}{2C'} + \frac{E_L}{2}\tilde{\phi}^2 + \frac{\epsilon}{2}\sigma_x + (E_J\cos\frac{\phi_{e1}}{2} - \frac{\tilde{\phi}}{2}E_J\sin\frac{\phi_{e1}}{2})\sigma_z. \tag{C.5}$$

where $\epsilon = 2e(e-q)/C_t = E_C(1-q/e)$.

The Hamiltonian in Eq. (C.5) describes a two-level system coupled to a harmonic oscillator. Hence, we can reduce the Hamiltonian to the two-level form by averaging over $\tilde{\phi}$, using the same arguments as in Sec. 4.1, provided that the plasma frequency is large, $\hbar\omega_p \gg E_J$, where $\hbar\omega_p = \sqrt{2E_C E_L}$. However, it is straightforward to show that this effect is small and that the two-level dynamics is determined by the Hamiltonian [66],

$$\hat{H} = E_J\cos\frac{\phi_{e1}}{2}\sigma_z + \frac{\epsilon}{2}\sigma_x. \tag{C.6}$$

The current operator averaged over the fluctuations of the harmonic oscillators is,

$$\hat{I}_l = \frac{2e}{\hbar}E_L\begin{pmatrix} \langle\tilde{\phi}\rangle_- & 0 \\ 0 & \langle\tilde{\phi}\rangle_+ \end{pmatrix} = \frac{I_c}{2}\sin\frac{\phi_{e1}}{2}\sigma_z \tag{C.7}$$

where $\langle\tilde{\phi}\rangle_\sigma$ is the average induced flux of the two qubit states.

The assumptions made for the charge-phase qubit can be written as a chain of inequalities,

$$E_J\cos\frac{\phi_{e1}}{2} \ll E_C, \hbar\omega_p, \hbar\omega_m \ll E_L, \tag{C.8}$$

where ω_m is the plasma frequency of the Meter.

BIBLIOGRAPHY

[1] Aconcagua, 6962m, is the highest mountain in America and located in the windy Andes between Argentina and Chile about 150km north of Santiago de Chile. The climbing is nice but the rock is loose.

[2] J. Bardeen, L. N. Cooper, and J. R. Schieffer, Phys. Rev. **108**, 1175 (1957).

[3] M. H. Cohen, L. M. Falicov, and J. C. Phillips, Phys. Rev. Lett. **8**, 316 (1962).

[4] B. D. Josephson, Phys. Lett. **1**, 251 (1962).

[5] B. Taylor and E. Burstein, Phys. Rev. Lett. **10**, 14 (1963).

[6] I. K. Yanson, V. M. Svistunov, and I. M. Dmitrnko, Sov. Phys. JETP **20**, 1404 (1965).

[7] G. I. Rochlin and D. H. Douglas, Phys. Rev. Lett. **16**, 359 (1965).

[8] J. R. Schrieffer and J. W. Wilkins, Phys. Rev. Lett. **10**, 17 (1963).

[9] N. N. Bogoliubov, Sov. Phys. JETP **34**, 41 (1958).

[10] P. G. D. Gennes and D. Saint-James, Phys. Lett. **4**, 151 (1963).

[11] A. F. Andreev, Sov. Phys. JETP **19**, 1228 (1964).

[12] L. N. Cooper, Phys. Rev. **104**, 1189 (1956).

[13] I. O. Kulik, Sov. Phys. JETP **30**, 944 (1970).

[14] J. Bardeen and J. L. Jonson, Phys. Rev. B **5**, 72 (1972).

[15] C. Ishii, Prog. Theor. Phys. **44**, 1525 (1970).

[16] A. V. Svidzinsky, T. N. Anzygina, and E. N. Bratus, J. Low Temp. Phys. **10**, 131 (1973).

[17] I. O. Kulik and A. N. Omel'yanchuk, Sov. J. Low Temp. Phys. **3**, 459 (1977).

[18] S. N. Artmenko, A. F. Volkov, and A. V. Zaitsev, Sov. Phys. JETP **49**, 924 (1979).

[19] W. Belzig, F. K. Wilhelm, C. Bruder, G. Schön and A. D. Zaikin, Superlattices and Microstructures **25 no. 5/6**, 1251 (1999).

[20] R. Landauer, IBM J. Res. Dev. **1**, 223 (1957).

[21] G. Blonder, M. Tinkham, and T. Klapwijk, Phys. Rev. B **25**, 4515 (1982).

[22] B. J. van der Wees *et al.*, Phys. Rev. Lett. **60**, 848 (1988).

[23] C. W. J. Beenakker, in *Solid State Physics* edited by H. Ehrenreich and D. Turnboll (Academic press, Inc., New York) **44**, (1991).

[24] T. M. Klapwijk, G. Blonder, and M. Tinkham, Physica B **109 and 110**, 1657 (1982).

[25] M. Octavio, M. Tinkham, G. Blonder, and T. M. Klapwijk, Physica B **27**, 6739 (1983).

[26] C. W. J. Beenakker and H. van Houten, Phys. Rev. Lett. **66**, 3056 (1991).

[27] A. Furusaki and M. Tsukada, Phys. Rev. B **43**, 10164 (1991).

[28] C. W. J. Beenakker, Phys. Rev. Lett. **67**, 3836 (1991).

[29] P. F. Bagwell, Phys. Rev. B **46**, 12573 (1992).

[30] V. S. Shumeiko, E. N. Bratus, and G. Wendin, Phys. Rev. B **48**, 13129 (1993).

[31] M. Hurd and G. Wendin, Phys. Rev. B **49**, 15258 (1994).

[32] L. Y. Gorelik *et al.*, Phys. Rev. Lett. **75**, 1162 (1995).

[33] G. B. Arnold, J. Low Temp. Phys **68**, 1 (1987).

[34] E. N. Bratus, V. S. Shumeiko, and G. Wendin, Phys. Rev. Lett. **74**, 2110 (1995).

[35] D. Averin and A. Bardas, Phys. Rev. Lett. **75**, 1831 (1995).

[36] J. C. Cuevas, A. Mart'in-Rodero, and A. Levy Yeyati, Phys. Rev. B **54**, 7366 (1996).

[37] E. N. Bratus, V. S. Shumeiko, E. V. Bezuglyi, and G. Wendin, Phys. Rev. B **55**, 12666 (1997).

[38] C. J. Muller, J. M. van Ruitenbeek, and L. J. Jongh, Physica C **191**, 485 (1991).

[39] C. J. Muller, J. M. van Ruitenbeek, and L. J. Jongh, Phys. Rev. Lett. **69**, 140 (1992).

[40] C. J. Muller *et al.*, Nanotechnology **7**, 409 (1996).

[41] M. A. Reed *et al.*, Science **278**, 252 (1997).

[42] H. Ohnishi *et al.*, Nature **395**, 780 (1998).

[43] A. I. Yanson *et al.*, Nature **395**, 783 (1998).

[44] E. Scheer *et al.*, Nature **394**, 154 (1998).

[45] M. C. Koops, G. V. van Duyneveldt, and R. de Bruyn Ouboter, Phys. Rev. Lett. **77**, 2542 (1996).

[46] H. Takayanagi, T. Akazaki, and J. Nitta, Phys. Rev. Lett. **75**, 3533 (1995).

[47] H. Nakano and H. Takayanagi, Solid State Commun. **80**, 997 (1991).

[48] H. Nakano and H. Takayanagi, Phys. Rev. B **47**, 7986 (1993).

[49] F. Hekking and Y. Nazarov, Phys. Rev. Lett. **71**, 1625 (1993).

[50] V. T. Petrashov *et al.*, Phys. Rev. Lett. **74**, 5268 (1995).

[51] A. Dimoulas *et al.*, Phys. Rev. Lett. **74**, 602 (1995).

[52] J. Kutchinsky, R. Taboryski, and J. B. Hansen, Phys. Rev. Lett. **74**, 602 (1997).

[53] J. Kutchinsky, R. Taboryski, and J. B. Hansen, Phys. Rev. B **56**, R2932 (1997).

[54] J. Kutchinsky *et al.*, Phys. Rev. Lett. **83**, 4856 (1999).

[55] R. Taboryski *et al.*, Superlattices and Microstructures **25**, 829 (1999).

[56] G. Wendin and V. S. Shumeiko, Phys. Rev. B **53**, R6006 (1996).

[57] P. Samuelsson, V. S. Shumeiko, and G. Wendin, Phys. Rev. B **56**, R5763 (1997).

[58] A. J. Legget, in *Chanse and Matter* edited by J. Souletie, J. Vannimenus and R. Stora (Elsevier, Amsterdam) 395 (1987).

[59] A. J. Legget, Rev. Mod. Phys. 59 (1987).

[60] J. R. Friedman *et al.*, Nature **406**, 43 (1999).

[61] C. P. Williams and S. H. Clearwater, *Explorations in quantum computing* (Springer-Verlag, New York, 1998).

[62] N. Gershenfeld and I. L. Chuang, Science **275**, 350 (1997).

[63] D. G. Cory and *et. al.*, Physica D **120**, 371 (1997).

[64] V. Bouchiat and *et. al.*, Phys. Scr. **T76**, 165 (1998).

[65] Y. Nakamura, Y. A. Pashkin, and J. S. Tsai, Nature **398**, 786 (1999).

[66] A. Cottet *et al.*, Physica C **367**, 197 (2001).

[67] J. Mooij and *et. al.*, Science **285**, 1036 (1999).

[68] Y. Makhlin, G. Schön, and A. Shnirman, Rev. Mod. Phys. **73**, 357 (2001).

[69] D. Vion *et al.*, *Manipulating the quantum state of an electric circuit* (unpublished) (2002).

[70] G. Johansson, G. Wendin, R. J. Schoelkopf, and P. Delsing, Phys. Rev. Lett. **86**, 3376 (2001).

[71] G. Johansson, A. Käck, and G. Wendin, Phys. Rev. Lett. **88**, 46802 (2002).

[72] A. Levy Yeyati, A. Mart'in-Rodero, and F. Flores, Phys. Rev. Lett. **71**, 2991 (1993).

[73] U. Eckern, G. Schön, and V. Ambeagaokar, Phys. Rev. B **30**, 6419 (1984).

[74] V. Ambegaokar and A. Baratoff, Phys. Rev. Lett. **10**, 486 (1963).

[75] V. Ambegaokar and A. Baratoff, Phys. Rev. Lett. **11**, 104(E) (1963).

[76] V. Ambegaokar, U. Eckern, and G. Schön, Phys. Rev. Lett. **48**, 1745 (1982).

[77] O. Zazunov, Ph.D. thesis, Chalmers University of Technology, 2002.

[78] W. Haberkorn, H. Knauer, and S. Richter, Phys. Status Solidi **47**, K161 (1978).

[79] K. K. Likharev and A. B. Zorin, J. of Low Temp. Phys. **59**, 347 (1985).

[80] D. V. Averin and K. K. Likharev, in *in Mesoscopic Phenomena in Solids* edited by B. L. Altshuler, P. A. Lee and R. A. Webb (Elsevier, Amsterdam) 173 (1991).

[81] A. V. Zaitsev and D. V. Averin, Phys. Rev. Lett. **80**, 3602 (1998).

[82] M. Büttiker, Phys. Rev. Lett. **57**, 1761 (1986).

[83] V. S. Shumeiko, E. N. Bratus, and G. Wendin, Low Temp. Phys. **23**, 181 (1997).

[84] G. Johansson, G. Wendin, V. S. Shumeiko, and K. N. Bratus, Superlattices and Microstructures **25**, 1115 (1999).

[85] G. Johansson, V. S. Shumeiko, E. N. Bratus, and G. Wendin, Phys. Rev. B **60**, 1382 (1999).

[86] B. Z. Spivak and D. E. Khemel'nitskii, JETP Lett. **35**, 412 (1982).

[87] C. J. Lambert and R. Raimondi, J. Phys.: Condens. Matter **10**, 901 (1998).

[88] T. Schäpers *et al.*, Appl. Phys. Lett. **73**, 2348 (1998).

[89] A. F. Morpurgo, T. M. Klapwijk, and B. J. van der Wees, Appl. Phys. Lett. **72**, 966 (1998).

[90] J. J. A. Baselmans, A. F. Morpurgo, B. J. van der Wees, and T. M. Klapwijk, Nature **397**, 43 (1999).

[91] B. J. van der Wees, K. M. H. Lenssen, and C. J. P. M. Harmans, Phys. Rev. B **44**, 470 (1991).

[92] L. F. Chang and P. F. Bagwell, Phys. Rev. B **55**, 12678 (1997).

[93] G. Wendin, V. S. Shumeiko, and P. Samuelsson, Swedish Patent application 9801614-6, 1998.

[94] G. Wendin and V. S. Shumeiko, Superlattices and Microstructures **20, no. 4**, 569 (1996).

[95] A. J. Legget and A. Garg, Phys. Rev. Lett. **54**, 857 (1985).

[96] A. Zazunov, V. S. Shumeiko, E. Bratus, J. Lantz and G. Wendin, *Andreev level qubit* (unpublished) (2001).

[97] M. H. Devoret, *Quantum fluctuations in electrical circuits* (Elsevier, Les Houches, Session LXIII, 1995, printed in 1997).

[98] U. Weiss, *Quantum Dissipative systems* (World Scientific, Singapore, 1999).

[99] M. E. Peskin, *Chapter 9 in* An Introduction to Quantum Field Theory (Addison-Wesley, New York, 1995).

[100] J. R. Friedman and D. V. Averin, Phys. Rev. Lett. **88**, 050403 (2002).

Paper I

Paper II

Paper III

Paper IV

Coherent processes in superconducting quantum interferometers and qubits

Jonn Lantz
Department of Microelectronics and Nanoscience
Göteborg University and
Chalmers University of Technology

ABSTRACT

In this thesis we present theoretical investigations of the effects of Andreev bound states on the current transport in superconducting interferometers. We also investigate the slow dynamics of the Andreev states in a superconducting point contact, and the possible application as a quantum bit.

We consider superconductor-normal metal-superconductor (SNS) and normal metal- superconductor (NS) interferometers, where the contact region is a Y-shaped normal metal wave guide, and the two connection points to the same superconducting electrode can have different phases. The electric current in the interferometer is calculated as a function of the applied voltage and the phase difference ϕ. Andreev reflection in SNS and NS interferometers incorporates two features: interference in the arms of the Y-shaped normal region, and interplay with Andreev resonances. The latter feature yields rich phase dependent current structures in the subgap voltage region. The interference effect leads to a suppression of the current structures at $\phi = \pi$.

We investigate the effects on the Josephson current in NS interferometers due to current injection from the normal electrode. The two main effects of the nonequilibrium situation are: nonequilibrium population of the Andreev levels, which can result in enhancement, suppression, or even sign reversal of the Josephson current, and an anomalous interference Josephson effect, which gives rise to a long range Josephson effect, increasing with the voltage eV up to the superconducting gap Δ.

The two Andreev states in a superconducting quantum point contact can be accessed for manipulation and measurement by embedding the point contact in a superconducting loop. We calculate an effective Hamiltonian for the slow dynamics of the Andreev two-level system in the ring. Furthermore, we discuss methods of manipulation of the Andreev levels, and coupling of qubits. The state of the Andreev two-level system can be read out by monitoring the macroscopic quantum tunneling in a current biased Josephson junction, which is embedded in the superconducting ring of the qubit. We discuss the effects on the qubit, the readout scheme and the signal-to-noise ratio.

Errata, Coherent processes in..., by J. Lantz, 2002

Page iii: Paper III is now published in Phys. Rev. B **65** 134523.

Page iii, Paper IV: the year should be 2002.

Page 12, Eq. 2.14: $D\phi_,$ should be $D\phi$ in both equations.

Page 13, Eq. 2.24: $\mathcal{V}_L$ should be $\mathcal{V}$.

Page 14, below Eq. 2.30: p_ϕ should be q_ϕ.

Page 23, Eq. 2.63: $J_{-n,j}(W)$ should be $J_{-n,j}(E)$.

Page 26, Citation [82] should be to M. Büttiker, Phys. Rev. Lett. **57**, 1761 (1986):

Page 27, Fig. 3.3: $S(\phi_d)$ should be $S(\phi)$.

Page 37, Eq. 4.3: $\frac{\partial \phi}{\partial \hat{H}}$ should be $\frac{\partial \hat{H}}{\partial \phi}$.

Page 40, above Eq. 4.15: "Rabi frequency" refers to the frequency of the Rabi oscillations.

Page 43, the text of Fig. 4.4: ϕ_3 should be ϕ_c.

Page 47, line 13: the reference to "beginning of this chapter" should be "Chapter 4".

Page 50, the first sentence: The time should be 23.59, Dec. 31 1999 instead of 00.00, Dec 31. :)